PHOTOLUMINESCENCE STUDIES OF THE YELLOW SERIES

FREE EXCITON IN CUPROUS OXIDE USING PULSED

AND CONTINUOUS WAVE TUNABLE DYE LASERS

by

ROBERT M. HABIGER

B.A., Bethany College, 1969

―――――――――

A MASTER'S THESIS

submitted in partial fulfillment of the

requirements for the degree

MASTER OF SCIENCE

Department of Physics

KANSAS STATE UNIVERSITY
Manhattan, Kansas

1975

Approved by:

Major Professor

TABLE OF CONTENTS

LIST OF FIGURES

ACKNOWLEDGEMENTS

INTRODUCTION

In 1931, J. I. Frenkel proposed the concept of the exciton for explaining absorption in solids that was not accompanied by photoconductivity.[1] This electrically neutral quasi-particle, consisting of an electron and hole bound through a Coulomb interaction, has the interesting property of being able to migrate through a crystal. The exciton can probably best be described in terms of two different limiting approximations, one due to Frenkel and the other due to Wannier and Mott. The Frenkel model considers the exciton tightly bound so that the electron and the hole are usually on the same atom in the lattice although they may migrate from atom to atom. In the Wannier model, the exciton is weakly bound so that the electron-hole separation may extend over many lattice constants. The particular model that is appropriate depends upon the state of the exciton and the properties of the insulator or semiconductor in which it is formed. A discussion of these two models is given in Knox's Theory of Excitons.[2]

Following Frenkel's fundamental work, the exciton hypothesis was used to explain various crystal phenomena. However, it was not until the early 1950's that systematic optical absorption experiments were performed by independent groups that confirmed the existence of excitons. Although nearly all semiconductors show exciton effects, cuprous oxide (Cu_2O) has a particularly rich optical spectrum and was therefore an important crystal in these early experiments. The first observations of exciton spectra were made by Hayashi.[3] Similar observations were made by Gross and Karryev a few months later and reported in 1952.[4] Gross had begun a study of the

optical absorption in Cu_2O at low temperatures in 1950 with the subsequent

observation of the hydrogen-like series at the absorption edge in 1951.

There are many excellent review articles on these early studies of excitons,

many of which discuss the particular properties of Cu_2O.[5-7]

Investigators have continued to show interest in the study of excitons

throughout the years and are now entering into a new field brought about

by the possibility of creating excitons at high densities. In fact H. Haken

and S. Nikitine have recently edited a book[8] devoted entirely to the dis-

cussion of topics involving excitons at high densities. In systems with

long exciton recombination lifetimes, such as in germanium, high density

effects can be seen at quite moderate excitation powers. But in other

semiconductors such as CdS, GaAs, CdSe, and Cu_2O with short exciton lifetimes,

high power pulsed laser excitation is often required to observe changes from

the usual (low density) photoluminescence spectra. But with high power

excitation, effects due to high exciton densities are often difficult to

identify with certainty because of the accompanying perturbations in the

phonon populations. These perturbations involve the creation of a large

number of optic or acoustic phonons. The resulting nonequilibrium phonon

population immediately following the laser pulse may be much greater than

that corresponding to the bath temperature and therefore have a significant

effect on the exciton energy distribution. This is discussed in more

detail and with appropriate references in the next section.

This thesis will present a study of the lowest state of the yellow

series exciton in Cu_2O under a wide range of incident laser power densities

and laser frequencies. A model involving the occurrence of exciton-exciton

scattering will be proposed to account for the observed effects at high

2

power densities. Using theoretical calculations and experimental observations, limits on the phonon populations can be made which rule out any possibility that the observed high density effects can be attributed to changes in these populations. Various lifetime estimates involving excitons and phonons can be made that are consistent with the proposed model. These will include lifetimes for exciton decay, phonon decay, exciton-exciton scattering, and exciton-acoustic phonon scattering.

A discussion of the experimental apparatus and procedures is included as well as comments on the difficulties characteristic of high power excitation studies.

Cuprous oxide has a simple cubic crystal structure with two molecules per unit cell. For the interested reader, band structure calculations are available in the literature.[9] The excitons of this semiconductor can be generally described by the Wannier model. Four different hydrogenic exciton series have been observed[7] with exciton radii as large as one hundred lattice constants for the higher excited states. This thesis will only be concerned with the yellow series which arises from direct gap transitions from the highest valence band (Γ_7^+) to the lowest conduction band (Γ_6^+). As pointed out by Elliott[10] this exciton has an overall symmetry of Γ_{25}^+ and is triply degenerate (ortho-exciton). Experiments indicating absorption line splitting in electric and magnetic fields have confirmed this degeneracy.[11] There should also exist a nondegenerate (para-exciton) with symmetry Γ_2^+. However its existence is not easily confirmed because an optical transition to this exciton state is forbidden in both the dipole and quadrupole approximations. Although the observation of this para-exciton has been reported in deformed crystals,[12] its exact energy relative to the ortho-exciton has not been substantially confirmed. In order for the conduction band electron and the valence band hole to bind together in an exciton, they must have equal velocities. This leads to the type of transition shown in Fig. 1a.

It is well known that excitons can possess a significant amount of kinetic energy. In fact, if the effective exciton mass is m*, then the total energy of the exciton is

$$E = E_G - \frac{\mu^* e^4}{2\hbar^2 \varepsilon^2 n^2} + \frac{\hbar^2 k_{ex}^2}{2m^*}$$

THIS BOOK
CONTAINS
NUMEROUS PAGES
THAT WERE
BOUND WITHOUT
PAGE NUMBERS.

THIS IS AS
RECEIVED FROM
CUSTOMER.

FIGURE 1

(a) The velocity of an electron or hole at a
particular point on an energy band depends
upon the slope of the band. This figure
shows a transition in which the hole and
electron have the same velocity thereby
giving rise to the possibility of forming
an exciton.

(b) Four different hydrogenic series of exciton
bands have been observed in Cu_2O. This
paper will only discuss the $n = 1$ band of
the yellow series.
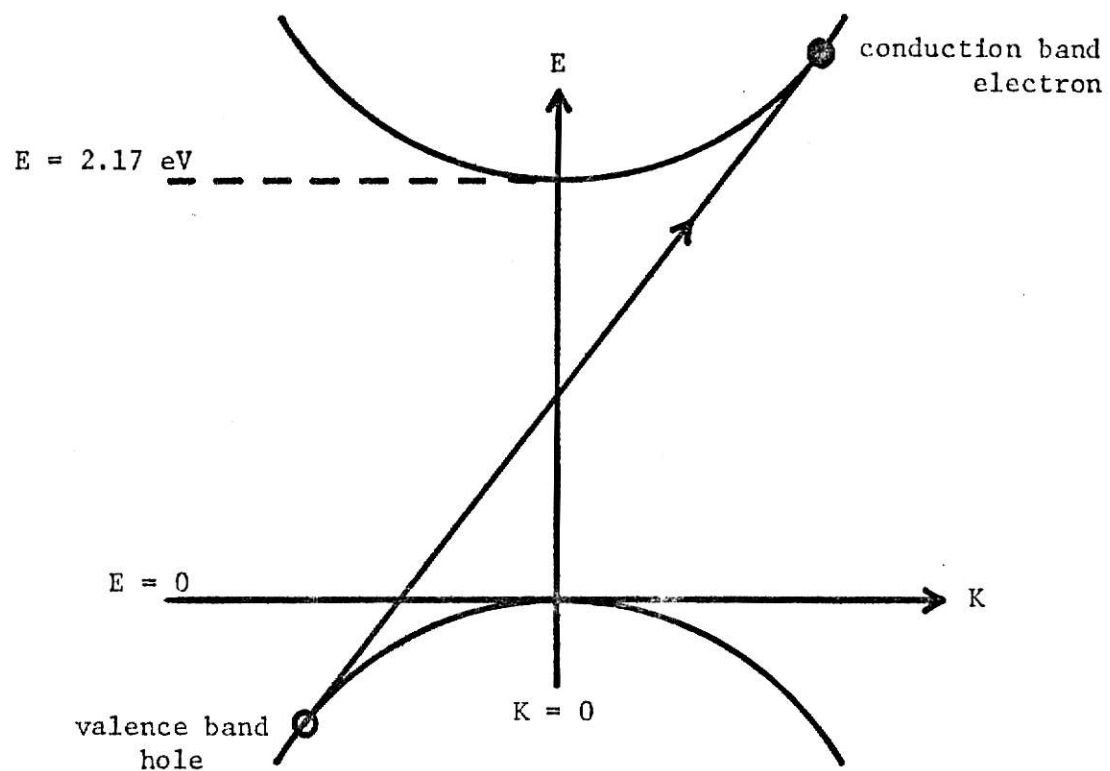
(a)
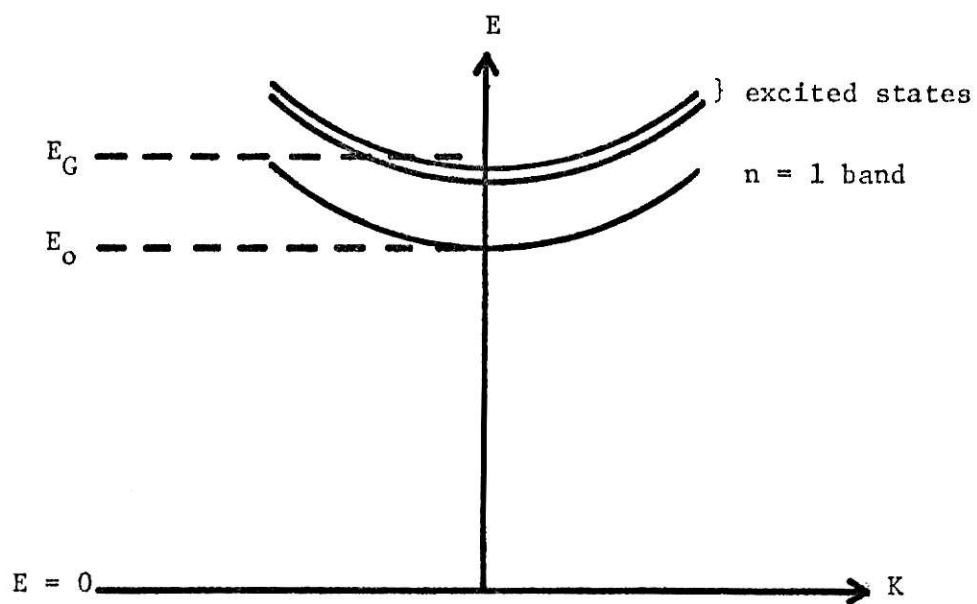
(b)

for direct gap materials. The exciton "Rydberg" is seen to be similar to the hydrogenic Rydberg constant. The reduced mass is replaced by the reduced effective masses of the hole and electron and the binding energy is reduced by the square of the dielectric constant ε. The second term is the kinetic energy which gives rise to an exciton band as shown in Fig. 1b. The bottom of the exciton band occurs at

$$E_o = E_G - E_B$$

so that the total energy of the exciton can be written

$$E = E_o + \frac{\hbar^2 k_{ex}^2}{2m^*} \quad . \tag{1}$$

The curvature of the exciton band is less than that for either the conduction or valence bands from which it is formed due to its larger effective mass. Although a value for the effective mass has not been firmly established, a recent report by Yu and Shen assign a value of three electron rest masses.[13]

Optical Absorption and Luminescence

In the creation of an exciton, both momentum and energy must be conserved. As is apparent in Fig. 2, it is impossible to create excitons with appreciable kinetic energy through just photon absorption since the small photon momentum would not allow momentum to be conserved. However it is possible to create excitons with a whole range of kinetic energies through a phonon-assisted absorption in which the photon energy goes into

FIGURE 2

An exciton with momentum $\hbar\vec{K}_{ex}$ and kinetic energy

$\dfrac{\hbar^2 K_{ex}^{\ 2}}{2m^*}$ cannot be created by a photon since energy

and momentum cannot be conserved.

E

Photon dispersion
curve

exciton

exciton
dispersion
curve

K

K_{ex}
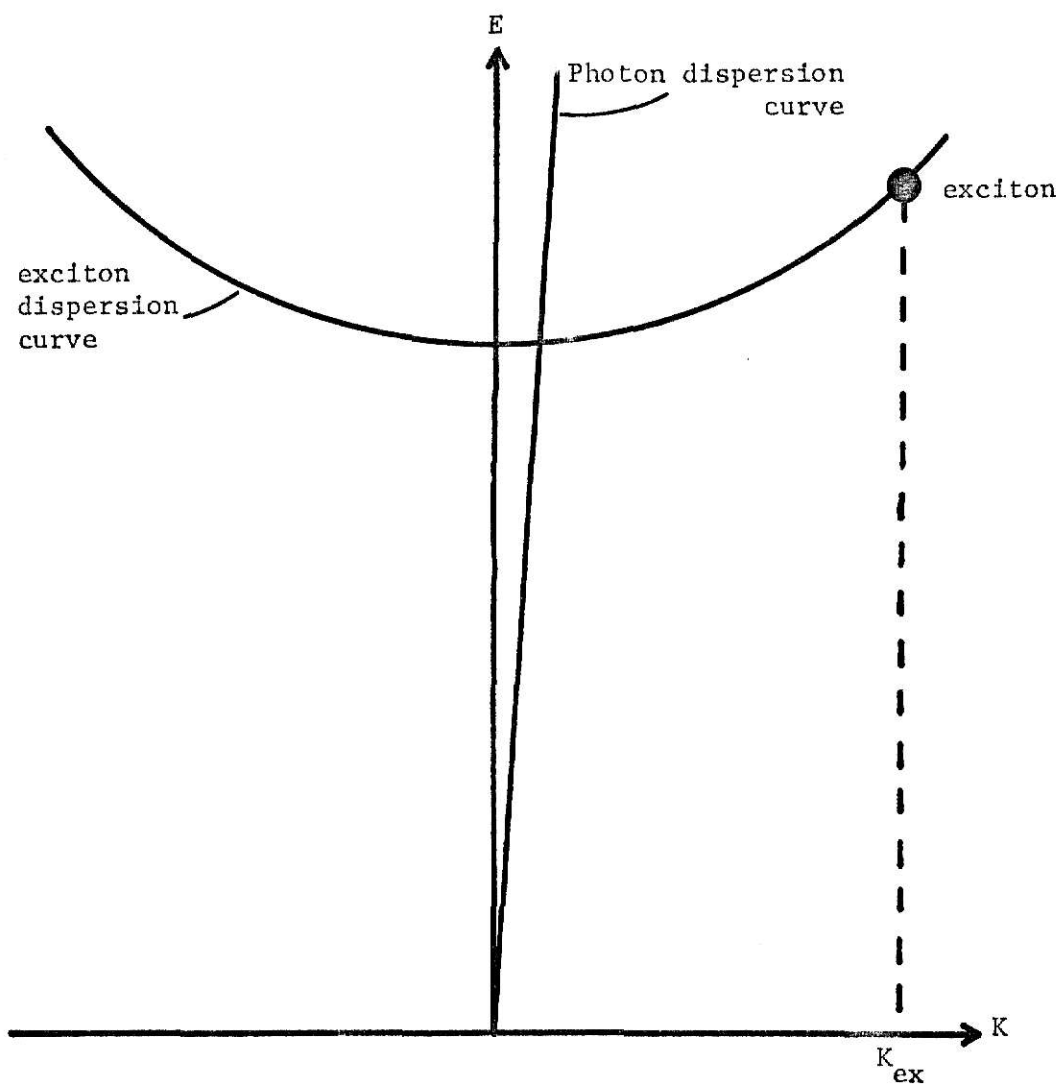
creating the exciton and an optic phonon. If $hc\bar{\nu}_i$ and $\hbar\vec{k}_i$ are the incident photon's energy and momentum, the conservation relations are

$$hc\bar{\nu}_i = hc\bar{\nu}_o + \frac{\hbar^2 k_{ex}^2}{2m^*} + E_o$$

(2)

$$\hbar\vec{k}_i = \hbar\vec{q} + \hbar\vec{k}_{ex}$$

where an optic phonon with energy $hc\bar{\nu}_o$ and momentum $\hbar\vec{q}$ is created in the absorption process. In the case of non-phonon-assisted absorption, excitons are created at the bottom of the band with essentially zero kinetic energy. This results in a sharp line that contributes to the hydrogenic series characteristic of Wannier excitons. However, in the case of Cu_2O this non-phonon-assisted absorption has electric quadrupole symmetry for the $n = 1$ band of the yellow series. In order for optical dipole transitions into this band to occur, they must be phonon-assisted with the strength of the transitions being determined by an *exciton-phonon coupling matrix element*. Since the Γ_{12}^- non-polar optic phonon couples most strongly with the exciton, any further discussion in this thesis concerning phonon-assisted transitions will be in reference to this particular phonon. Based upon an understanding of the exciton band and the phonon-assisted process, it is now possible to predict the functional form for absorption and luminescence involving the $n = 1$ band of the yellow series.

From time dependent perturbation theory, the coefficient for phonon-assisted absorption into the $n = 1$ exciton band is given by

$$\alpha(\bar{\nu}_i) = \frac{2\pi}{\hbar}|<f|v|i>|^2 D(E)$$

10

where $\bar{\nu}_i$ is the frequency of the incident photon and E is the exciton energy defined in Eq. (1). The exciton-phonon coupling matrix element is independent of the phonon wave vector[14] so that the momentum dependence of the absorption constant arises only from the density of final states. Due to the essentially dispersionless nature of the Γ_{12}^- phonon, the final density of states is just the exciton density of states. Using the spherical band approximation this density of states can be easily calculated for a sample of volume $V = (L_x)(L_y)(L_z)$.

$$D(E) = \frac{dN}{dk}\frac{dk}{dE}\Big|_{k=k_{ex}}$$

where

$$N = \frac{4\pi k^3}{3} \div (\frac{2\pi}{L_x})(\frac{2\pi}{L_y})(\frac{2\pi}{L_z}) \qquad \text{and} \qquad E = E_o + \frac{\hbar k_{ex}^2}{2m^*} \quad .$$

The result is

$$D(E) = 2V[\frac{m^*}{\hbar}]k_{ex}$$

$$= 2\pi V[\frac{2m^*}{\hbar}]^{3/2}(hc\bar{\nu}_i - hc\bar{\nu}_o - E_o)^{1/2}$$

where the conservation of energy relation from Eq. (2) was applied for the final result. The density of states therefore gives rise to a phonon-assisted absorption edge that occurs at $hc\bar{\nu}_i = hc\bar{\nu}_o + E_o$ and increases as the square root of the energy above the edge. Figure 3 shows an absorption spectrum taken at 20K. The quadrupole non-phonon-assisted line is too weak to be

FIGURE 3

Shown is experimental data for the Cu_2O absorption

constant as a function of frequency at 20K.
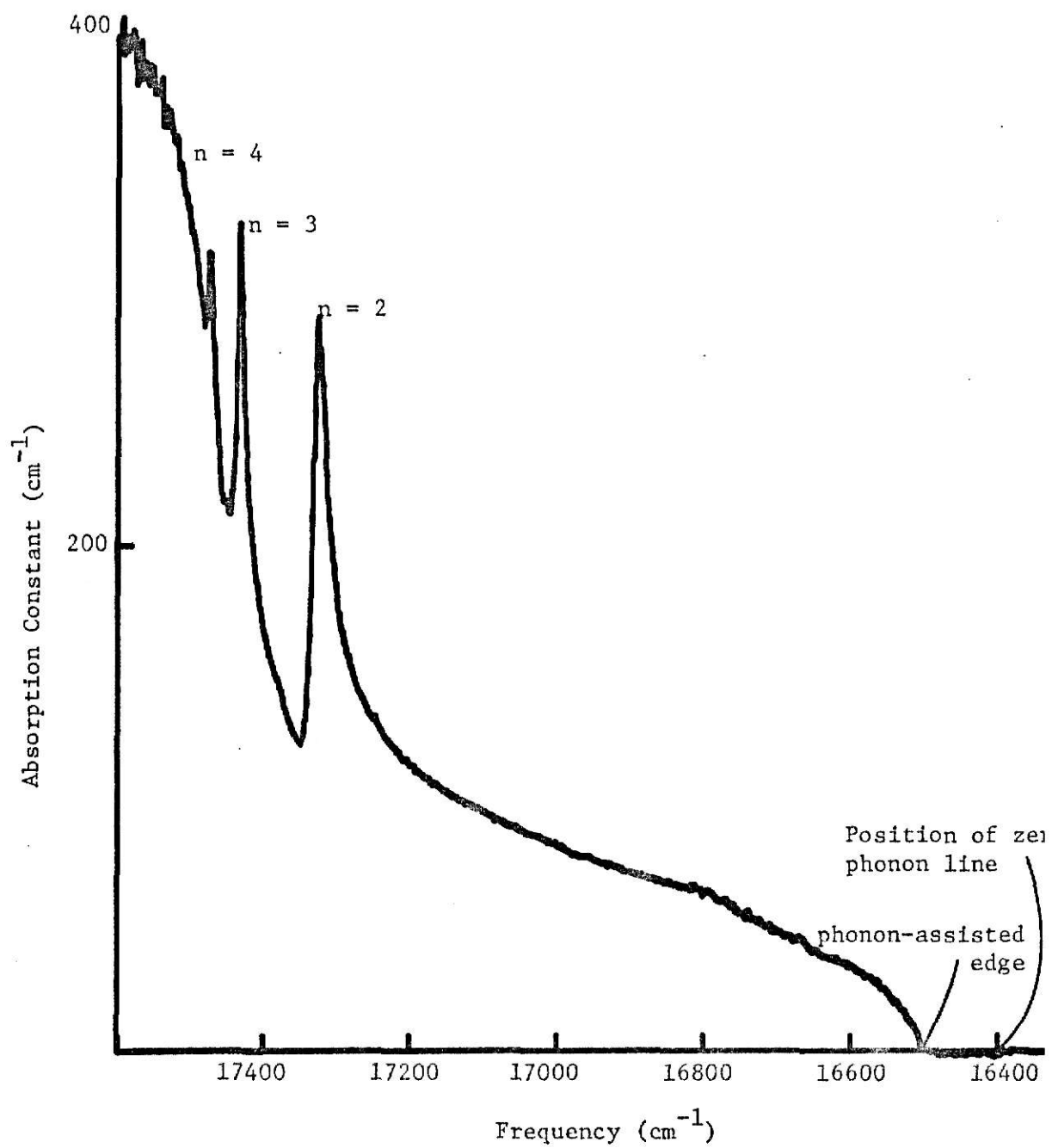
seen in this data, however the n = 2, n = 3, and n = 4 lines of the hydrogenic series are clearly evident.

In a similar way the luminescence intensity can be determined from time dependent perturbation theory. The transition probability from an initial exciton state of momentum $\hbar\vec{k}_{ex}$ and kinetic energy $\dfrac{\hbar^2 k_{ex}^2}{2m^*}$ to a final state consisting of a photon and a Γ_{12}^- phonon is given by

$$\frac{2\pi}{\hbar} D_f(E) \left| <f|v|i> \right|^2 \quad .$$

To get the total transition probability, it is necessary to sum over the exciton states with momentum $\hbar\vec{k}_{ex}$ and kinetic energy $\dfrac{\hbar^2 k_{ex}^2}{2m^*}$ which are initially populated.

$$D_{ex}(k_{ex}) n(k_{ex}) \frac{2\pi}{\hbar} D_f(E) \left| <f|v|i> \right|^2$$

For the luminescence process, the momentum and energy conservation relations become

$$hc\bar{\nu}_p = \frac{\hbar^2 k_{ex}^2}{2m^*} - hc\bar{\nu}_o + E_o$$

$$\hbar\vec{k}_{ex} = \hbar\vec{k}_p + \hbar\vec{q}$$

where $hc\bar{\nu}_p$ and $\hbar\vec{k}_p$ are the energy and momentum of the luminescing photon. These relations uniquely determine the final state so that the density of final states in one. Repeating the density of exciton states calculation for the new conservation relations and using Bose-Einstein statistics for

the occupation probability $n(k_{ex})$ results in

$$I(\Delta E) = \frac{I_o (\Delta E)^{1/2}}{[\exp(\frac{\Delta E - \mu}{kT^*}) - 1]} \qquad \Delta E = hc\bar{\nu}_p - (E_o - hc\bar{\nu}_o) \qquad (3)$$

The matrix element has been absorbed into the constant I_o because of its independence of wave vector. T^* is the "effective temperature" of the exciton system and may or may not be equal to the lattice temperature. Figure 4a shows how the density of states is folded with the Bose-Einstein factor to form the phonon sideband described by Eq. (3). ΔE is the energy measured from the phonon sideband edge which is at 16285 cm^{-1} for 20K. Non-phonon-assisted luminescence exists in the form of a weak line which can be seen in the spectrum of Fig. 4b. This quadrupole feature is commonly referred to as the "n = 1 line" or the "zero-phonon line."

In practice it is possible to replace the Bose-Einstein factor with the classical Boltzmann distribution factor for the exciton densities and temperatures involved in these experiments. For example, a classical description would certainly be applicable if the mean separation between excitons is much greater than their de Broglie wavelength. The mean exciton separation $\bar{R}$ can be approximated by imagining each exciton to occupy a small cube of side R so that N of them fill the volume V. $\bar{R}$ is then given by

$$\bar{R} = (\frac{V}{N})^{1/3} \quad .$$

The de Broglie wavelength can be estimated for a thermal exciton at temperature T as

15

FIGURE 4

(a) The phonon sideband is found by the folding
of the density of states with a statistical
distribution factor.

(b) This luminescence spectrum of Cu_2O demonstrates
the phonon sideband.

Density of states

Composite Curve

Exponential

E

(a)

Zero-phonon line

E

(b)

17
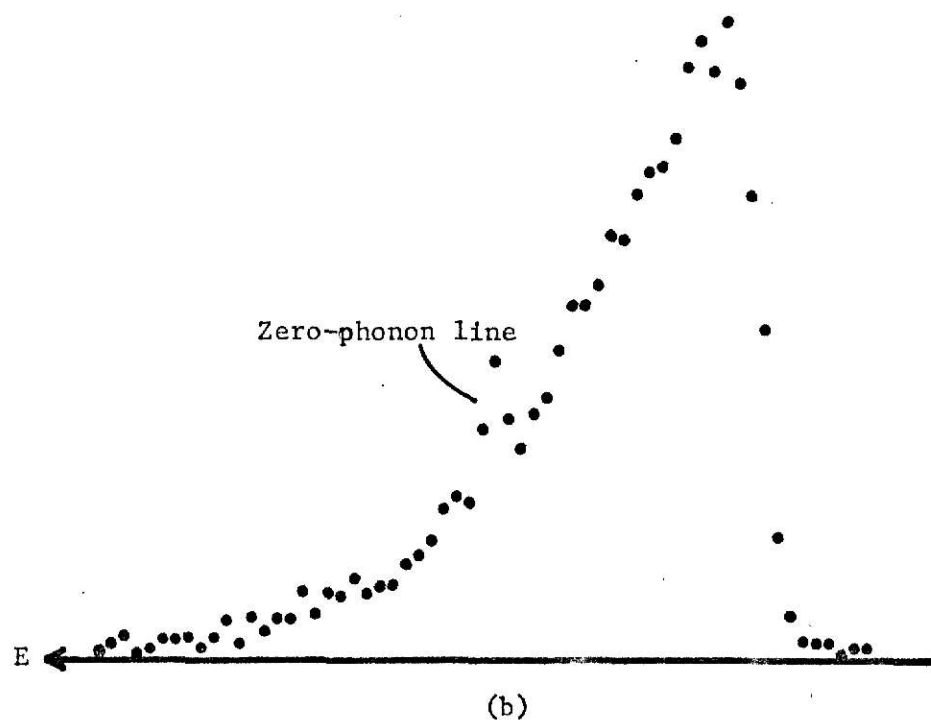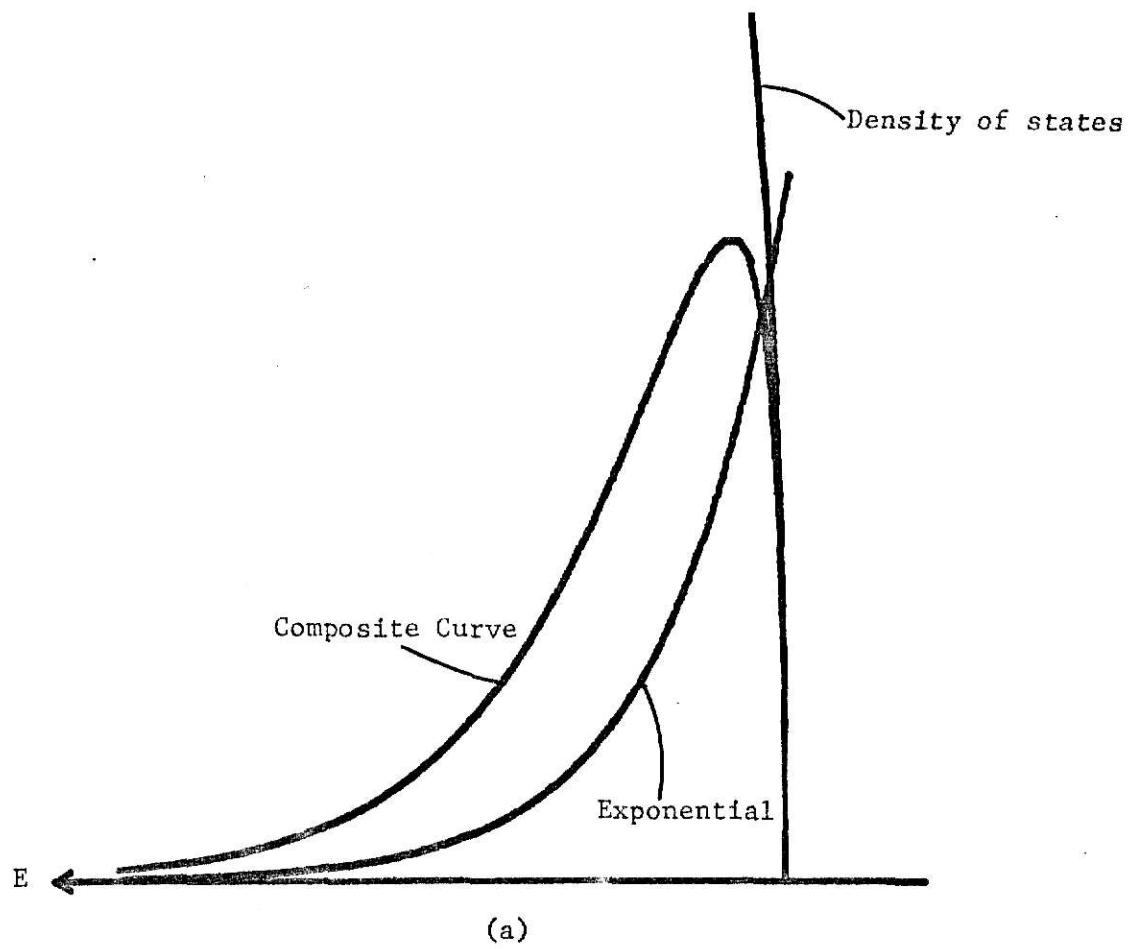
$$\bar{\lambda} = \frac{h}{p} = \frac{h}{[3m*kT*]^{1/2}} \quad .$$

Then applying the requirement $\bar{R} >> \bar{\lambda}$ means that

$$\frac{N}{V} << [\frac{3m*kT*}{h^2}]^{3/2} \quad .$$

For the experiments described in this paper, the most severe test of this criteria occurs for a density of 4.5×10^{17} cm^{-3} and an exciton temperature of 65K. Under these conditions

$$\frac{N}{V} = 4.5 \times 10^{17} \text{ cm}^{-3} \quad \text{and} \quad [\frac{3m*kT*}{h^2}] = 22 \times 10^{17} \text{ cm}^{-3} \quad .$$

Another method of evaluating the applicability of Boltzmann statistics is to compute the chemical potential. For a given temperature and density, the chemical potential is determined by the requirement that the total number of particles in the system comes out correctly. The defining relation is therefore

$$N = \int D(E)n(E)dE \quad .$$

Using the exciton density of states calculated earlier and the Bose-Einstein occupation probability leads to

$$\frac{N}{V} = 2\pi \left(\frac{2m^*}{h^2}\right)^{3/2} \int_0^\infty \frac{E^{1/2}dE}{\exp[(E-\mu)/kT^*]-1}$$

$$= \left[\frac{2\pi m^* kT^*}{h^2}\right]^{3/2} \sum_{n=1}^\infty \frac{e^{n\mu/kT^*}}{n^{3/2}} \quad .$$

For $N/V = 4.5\times10^{17}$ cm^{-3} and $T^* = 65$K this becomes

$$\sum_{n=1}^\infty \frac{e^{n\mu/kT^*}}{n^{3/2}} = 6.87\times10^{-2} \quad .$$

Solving this relation numerically produces a value for μ which is 122 cm^{-1} below the bottom of the exciton band.

Although the applicability of Boltzmann statistics is not rigorously supported, the approximation is certainly good enough for the type of curve fits made in this paper. It is then possible to replace Eq. (3) with

$$I(\Delta E) = b(\Delta E)^{1/2} \exp\left(\frac{-\Delta E}{kT^*}\right) \tag{4}$$

with the effective temperature T^* and the normalization constant b treated as parameters to be determined by the best fit to the data. In this way a temperature for the exciton system can be established which reflects its kinetic energy distribution.

Exciton Interactions

From this distribution it is possible to gather information about the

kinetics of exciton interactions with themselves and with the lattice. It is also possible to make an estimate of the exciton lifetime relative to these other processes. As was seen earlier, excitons may be created through phonon-assisted absorption with kinetic energies that well exceed the lattice thermal energy. Because the exciton system is in thermal contact with the lattice via exciton-phonon interactions, the excitons will attempt to reach a thermal equilibrium with the lattice through phonon relaxation. If complete thermalization is achieved, then Eq. (4) will describe the luminescence quite accurately with T* being the lattice temperature. In many semiconductors the most probable relaxation process is the emission of longitudinal optic (LO) phonons. However in order for complete thermalization with the lattice to occur, there must be multiple interactions with acoustic phonons, including both emission and absorption. In materials with very short exciton lifetimes this complete thermalization may not occur. The result is "hot" exciton luminescence.[15] The degree to which the excitons thermalize to the lattice temperature provides an indication of the exciton lifetime relative to the exciton-acoustic phonon relaxation time. Exciton temperatures that are 10 to 20 degrees above the lattice temperature have been reported by independent groups on various semiconductors.[14,16] Gross et al., have reported sharp emission lines in CdS[17] and CdSe[18] that are shifted in energy by integer numbers of LO phonons from the laser line which they attribute to hot exciton luminescence.

When low power density laser excitation is used, the formation of hot excitons is governed mainly by their interaction with phonons. Another method of creating a nonequilibrium system is by producing large exciton densities so that exciton-exciton collisions enable the kinetic energy

20

equilibration to take place within the exciton subsystem faster than between excitons and the lattice.

As mentioned earlier, high density exciton systems may also give rise to many other interesting effects. The formation of bi-excitons has been reported by different groups in a variety of materials[8] including CuCl, CuBr, CdS, CdSe, Ge, Si, and even Cu_2O. However, not all of these observations have been confirmed. For proper values of exciton concentration and temperature there exists the possibility of forming a Bose-condensation for which the excitons will all occupy the ground state of the exciton system. There have been many attempts to observe a Bose-condensation but the results are not yet conclusive. Condensation of bi-excitons has been reported in CdSe[19] although those results have been questioned.[20] Bose-condensation has also been reported for free excitons in AgBr.[21] Another interesting phenomenon that occurs for a sufficiently high excitation intensity is stimulated emission from excitons. In the case of CdS, the population inversion is between an exciton level and a lattice vibrational sublevel so that the emission involves the creation of a photon and an LO phonon.[22] Haken and Nikitine's book[8] presents a nice discussion of stimulated emission from excitons including both theory and experimental observations.

In most materials the creation of energetic, high density systems of excitons results in a large population of free carriers. If created in sufficient density these free carriers will thermalize among themselves in the same manner as excitons. Shah[16] has reported free carrier temperatures of 140K at a bath temperature of only 2K for CdSe. A large concentration of hot carriers can cause a significant effect on the high energy tail of exciton luminescence because of exciton-free carrier collisions. It is

also possible that under high laser power excitation a nonequilibrium distribution of phonons is created which will affect the exciton features. Long term changes in phonon populations arising from crystal heating can be easily identified as will be seen later in this paper. However, as pointed out by Shah, Leheny, and Brinkman,[23] perturbations to these populations on a nanosecond time scale are not always easily detectable. A recent report[24] on the radiative emission spectrum of CdS under high intensity excitation suggests effects arising from both a large density of hot electrons and a nonequilibrium distribution of optic phonons.

It is therefore necessary to proceed with caution in making studies of exciton luminescence spectra under high intensity excitation. However Cu_2O has some advantageous characteristics over other materials that make the study of hot exciton effects easier. Because of the dispersionless nature of the Γ_{12}^- phonon and its strong coupling to the exciton, it is possible to pump directly into the exciton band using a tunable dye laser. Further, the relatively large binding energy makes it possible to create excitons with quite large kinetic energies without the problem of creating an excess of free carriers. The large binding energy and excitonic Rydberg enables one to study elastic scattering effects over a wide range of kinetic energies. The binding energy for the n = 1 exciton in Cu_2O is about .14 eV compared to the approximate values of .03 eV for CdS, .015 eV for CdSe, .003 eV for GaAs, and .005 eV for Ge.

EXPERIMENTAL CONSIDERATIONS

Two different lasers were used in performing the experiments presented in this paper. A continuous wave (CW) laser was used to produce very low density exciton systems and a pulsed laser was used to produce high density exciton systems.

The CW laser system consisted of an argon ion laser pumping a tunable dye laser, both manufactured by Coherent Radiation. The dye used was Rhodamine 6G which has a rated tuning range of approximately 5700-6100 angstroms. However, the power of the dye laser falls off very rapidly in the wings of the tuning range and it was necessary to add small amounts of 1, 3, 5, 7-Cyclooctatetraene (COT) to the dye solution in order to lase far enough into the red as required by some experiments. Broadband dye fluorescence was a particular problem since it gave rise to a background signal that competed successfully with the exciton luminescence. A 600 lines/mm diffraction grating was generally used in conjunction with a ~3 mm diameter aperture at a distance of 1.9 meters for rejecting this background fluorescence. For some experiments, a constant deviation prism was used in lieu of the grating although its dispersion is not as large as that of the grating.

The pulsed laser was a Molectron system consisting of a pulsed nitrogen laser pumping a tunable dye laser. The laser could be operated at eight different pulse repetition rates in the range from 5 to 50 pulses per second. Most of the data was taken at 25 pulses per second. The peak output of the nitrogen laser is rated at 1 megawatt and the peak output of the dye laser is rated at 100 kilowatts for Rhodamine 6G. However, a major limitation

of the pulsed laser system was the onset of surface damage to the sample at high power densities so that peak powers of not more than approximately 40 kilowatts were actually required. The optical system for positioning and focussing the beam on the sample is shown in Fig. 5. The cylindrical lens (f = 12.3 cm) produced a line focus which allowed a maximum amount of light into the slits of the spectrometer without creating surface damage. The spherical lens (f = 40 cm) was adjusted to produce the desired line length. Fine adjustment of the mirror mount was accomplished with micrometer barrels so that the line could be positioned precisely on the sample. Although at the ends of the dye tuning range the peak power of the dye laser was considerably lower than 40 kW, the limiting factor on the power densities attainable was still the surface damage. The full pulse width at half maximum was approximately 7 nanoseconds. Three different dye solutions were used in order to cover the spectral range desired. Rhodamine B (5940 - 6430 angstroms), Rhodamine 6G (5680-6050 Angstroms), and a mixture of 4% Rhodamine B and 96% Rhodamine 6G were used to scan with sufficient power the range from near the bottom of the exciton band to above the band gap. Two prisms in conjunction with a 0.6 cm aperture located at 2.1 meters were used to reduce the dye fluorescence.

The detection system consisted of a Spex 1401 double grating spectrometer and photon counting electronics. The photomultiplier tube was an ITT FW 130 with an S-20 cathode. It was cooled to approximately 253K in order to lower the dark count. A calibration of the spectral throughput for the spectrometer and photomultiplier tube was performed with the results shown in Fig. 6.

FIGURE 5

Schematic diagram of the optical system for focussing
and positioning the laser beam on the sample.

Mirror
Mount

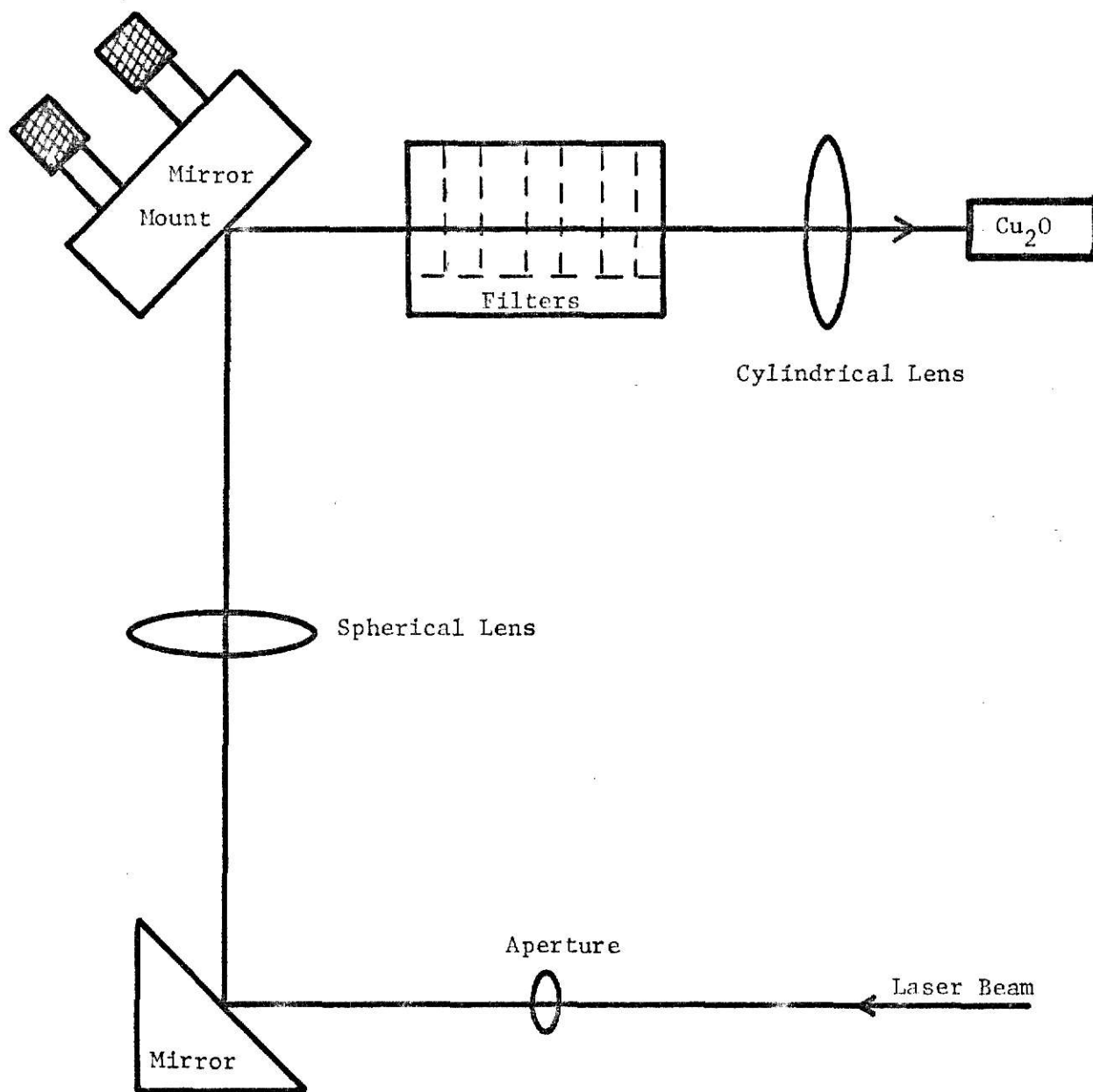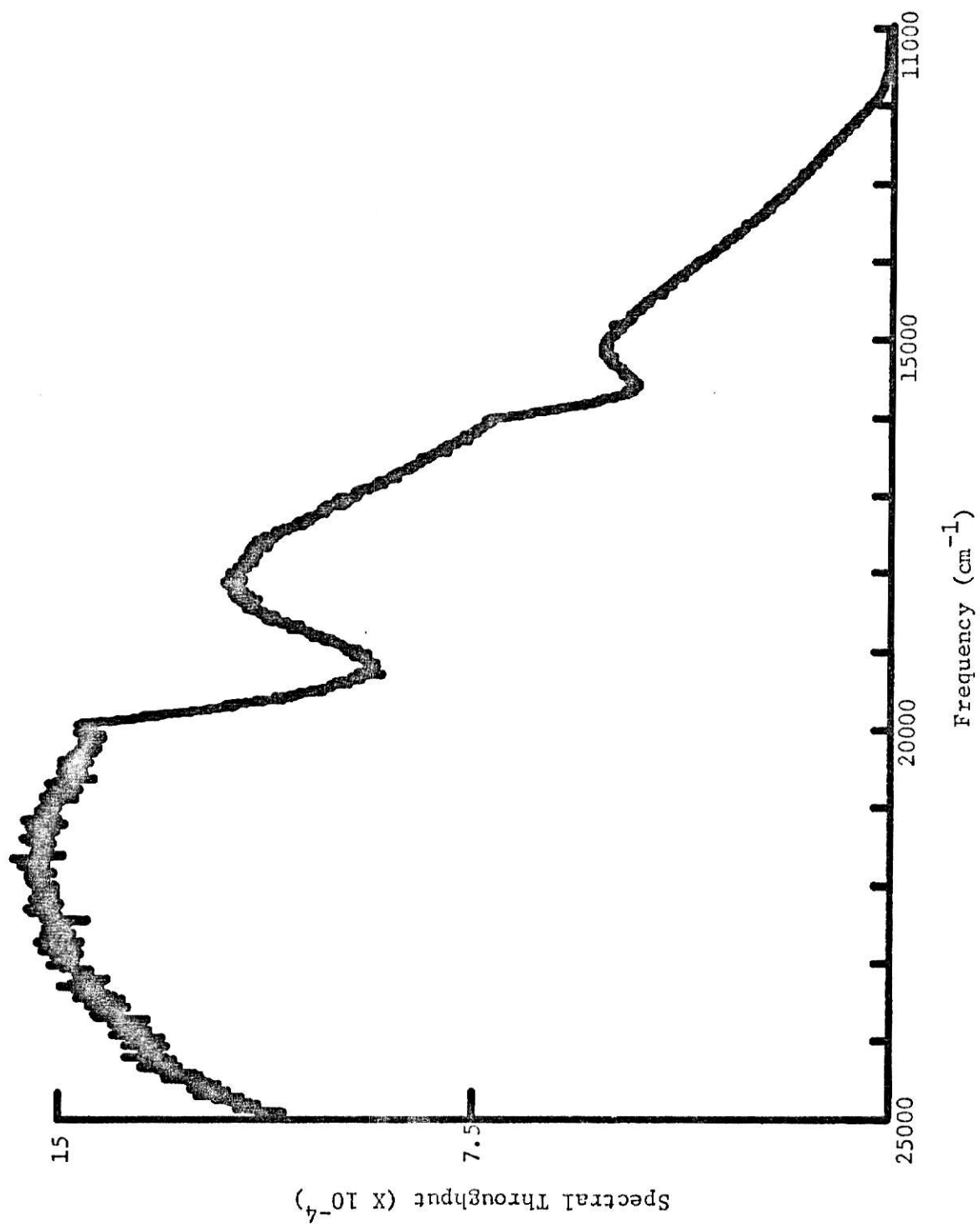Filters

Cylindrical Lens

Cu_2O

Spherical Lens

Aperture

Laser Beam

Mirror

FIGURE 6

Spectral throughput of the spectrometer and photomultiplier tube for an
unpolarized light source.

Frequency (cm^{-1})

Spectral Throughput (X 10^{-4})

The type of photon counting electronics used depended upon whether the CW or the pulsed laser was being used. An existing, standard photon counting arrangement was used with the CW laser. A block diagram of the components is shown in Fig. 7. The counting circuit portion of the system consisted of a Hewlett Packard 5326C frequency counter and a counting interval circuit. The frequency counter was operated in a manner that displayed the number of pulses received from the photomultiplier tube during a selected counting interval. This number was then recorded on paper tape.

The signal with the CW laser was generally well over an order of magnitude above the photomultiplier tube dark count of ten counts per second so that the dark count provided no real problem. But in the case of the pulsed laser, the dark count posed a significant problem. Although many luminescent and scattered photons may be generated by a single laser pulse, the photon counting system can detect at most only one event per laser pulse since all events fall within the resolving time of the photo-multiplier tube (~20 nanoseconds). Since multiphoton events recorded as single photon events would have greatly distorted the data, it was necessary to attenuate the signal entering the spectrometer to a level where multiphoton events were unlikely. For a pulse repetition rate of 25 pulses per second, the signal had to be attenuated to give a maximum of approximately 12 counts per second which posed a real problem since the dark count was around 10 counts per second. The solution was to construct a gated photon counting system, a block diagram of which is shown in Fig. 8. The gated photon counting technique is desirable because it essentially eliminates the photomultiplier tube dark count which would

FIGURE 7

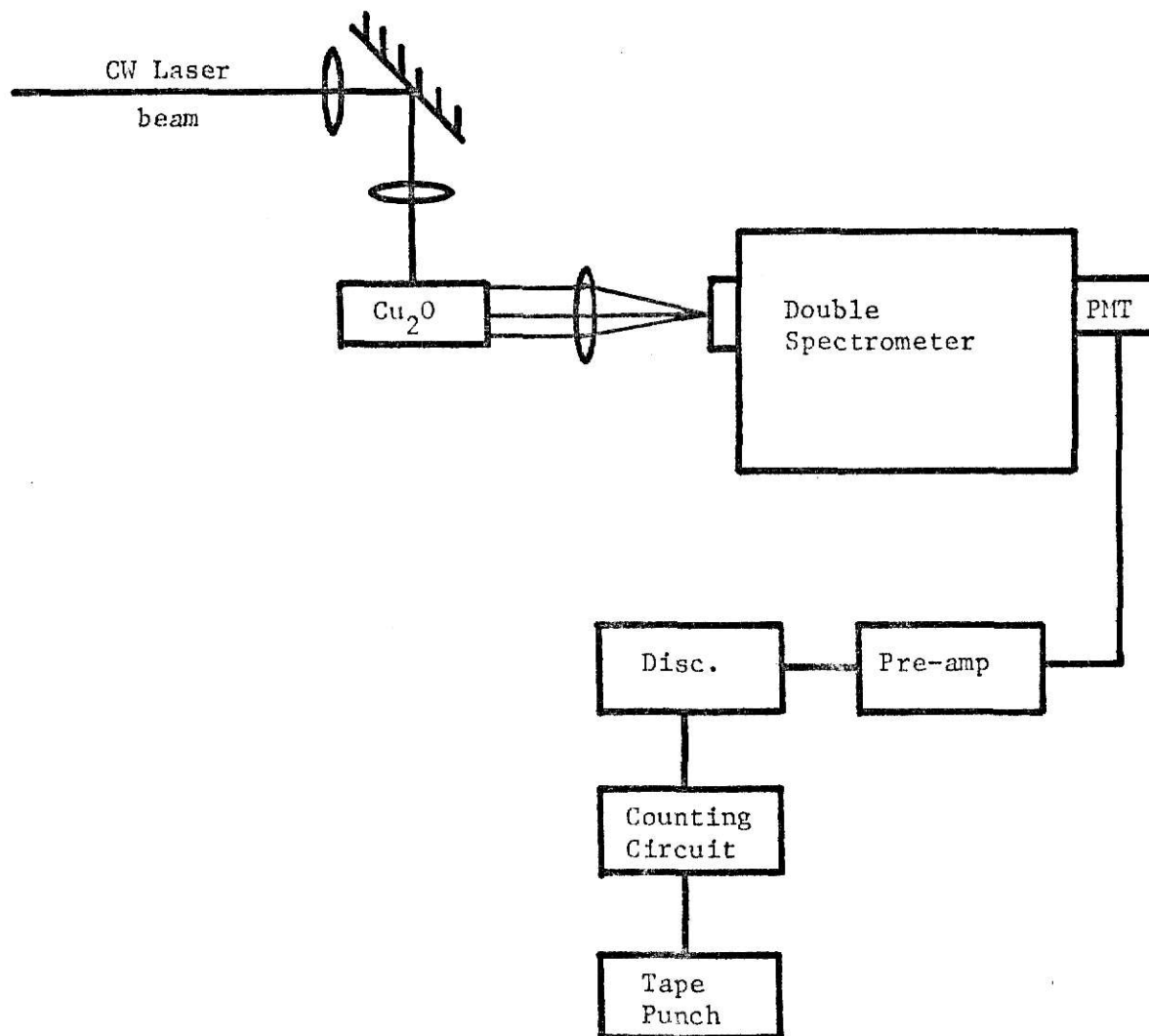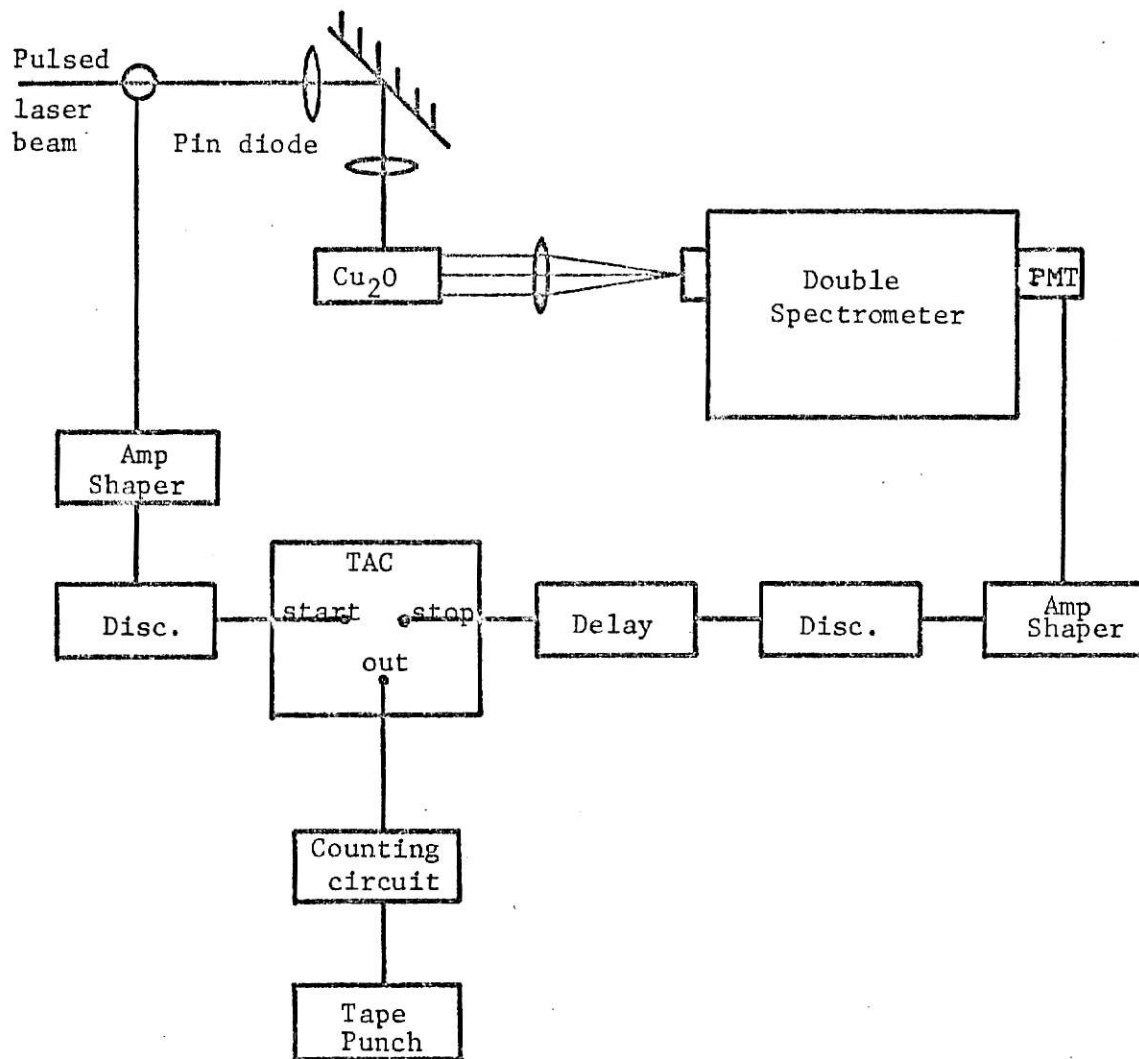Detection system for the CW laser experiments.

FIGURE 8

Detection system for the pulsed laser experiments.

otherwise be a problem for low signal levels. For example, the ITT FW 130 tube used in these experiments was operated at between 1750 and 1900 volts for which the dark count was less than 20 counts per second. By using a gate width of 50 nanoseconds, the gated dark count becomes less than

$$(20 \text{ cts/sec})(50 \times 10^{-9} \text{ sec})(25 \text{ gate triggers/sec}) = 2.5 \times 10^{-5} \text{ cts/sec}.$$

However, only the random noise can be eliminated in this fashion. Any noise that is correlated with the laser pulse and occurs within the gated interval is not eliminated. This noise must be eliminated by raising the discriminator level and by careful shielding. This problem will be discussed later in this section. With no dark count it was then only necessary to increase the counting time for each data point in order to achieve reasonable statistics. The data presented in this paper was taken using a counting time of 40 seconds per data point. The time-to-amplitude converter (TAC) used with the pulsed laser was set for a range of 50 nanoseconds. Since the luminescent signal followed the laser pulse by less than 10 nanoseconds,[†] the TAC acted very nicely as a simple gate generator.

Even though the signal pulse rate was kept less than half the laser repetition rate, it was still necessary to apply a statistical correction factor to the raw data to account for the possibility of more than one photon being generated by a single laser pulse. A correction of this type has been pointed out by J. I. Levatter et al.[25] This correction has been applied to all the pulsed laser data presented in this paper and it is

---

[†]This is known as a result of luminescence lifetime measurements which are discussed later in this paper.

summarized below for the convenience of the reader.

N = average number of photons generated per laser pulse

n = average number of photons reaching the detector per laser pulse

r = n/N = <u>a priori</u> probability that any one photon will reach the detector

Then the probability that any one photon does not reach the detector is $(1 - r)$. The probability that all N photons do not reach the detector is $(1 - r)^N$. Finally, the probability that at least one photon reaches the detector out of N generated in one laser pulse is

$$R = 1 - (1 - r)^N \quad .$$

But R is just what we observe experimentally since

$$R = \frac{\text{number of counts observed}}{\text{number of pulses}}$$

$$= 1 - (1 - n/N)^N \sim 1 - e^{-n} \text{ for large N}$$

$$e^{-n} = 1 - R$$

$$n = -\ln(1 - R) \quad .$$

The approximation made in going from $1 - (1 - n/N)$ to $1 - e^{-n}$ is very good since typically $n/N \sim 10^{-6}$ and $N \sim 10^8$. So it is possible to calculate the "true" average number of photons reaching the detector (n) as a function of the apparent number of photons reaching the detector (R). The validity of this correction depends on the accuracy of the defined probabilities, the

most questionable being R. Since the reliability of any probability interpretation increases with a larger number of samples, it is clear that the above argument becomes better as the number of laser pulses increases. This of course requires longer counting times. In the experiments presented in this thesis, the determination of R was based upon a sampling of

$$(25 \text{ pulses/sec}) \times (40 \text{ sec}) = 1000 \text{ pulses} \quad .$$

The setting of the discriminators for both laser systems was very important. They had to be set high enough so that most of the electrical noise was rejected but not so high as to discriminate against single photon events in favor of multiphoton events. Plots of the differentiated signal verses discriminator settings for both systems is shown in Fig. 9. Noise pulses have a distribution of pulse heights that is generally weighted with smaller pulses. The number of pulses with pulse heights in a given discriminator range is therefore quite large for small discriminator values but decreases fairly rapidly with increasing settings. As the region of single photon events is approached, the number of pulses in the given range increases to a maximum at the center of the single photon distribution and then decreases again resulting in the peaks that are seen in Figs. 9(a) and 9(c). The discriminator setting is then chosen which serves as a compromise between allowing a maximum number of single photon events while rejecting most of the dark count. This setting was especially critical for the pulsed laser system. The pulsed laser generated a significant amount of noise that was picked up by the pulse counting electronics.

36

FIGURE 9

Differentiated spectra of detected counts verses discriminator settings is shown for:

(a) a continuous light source with the CW laser system.

(b) the dark count spectrum of the CW laser system.

(c) a continuous light source with the pulsed laser system.

(d) the dark count spectrum of the pulsed laser system.

(a)

discriminator setting

(b)

(c)

discriminator setting

(d)
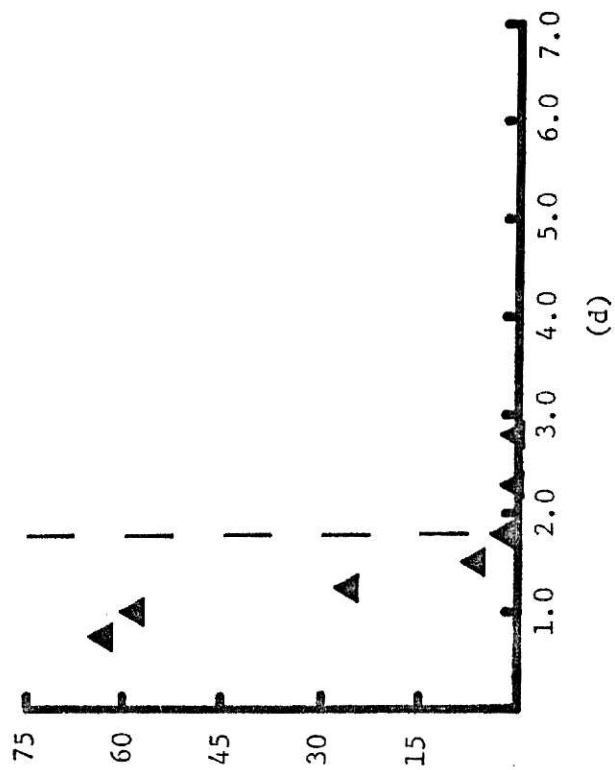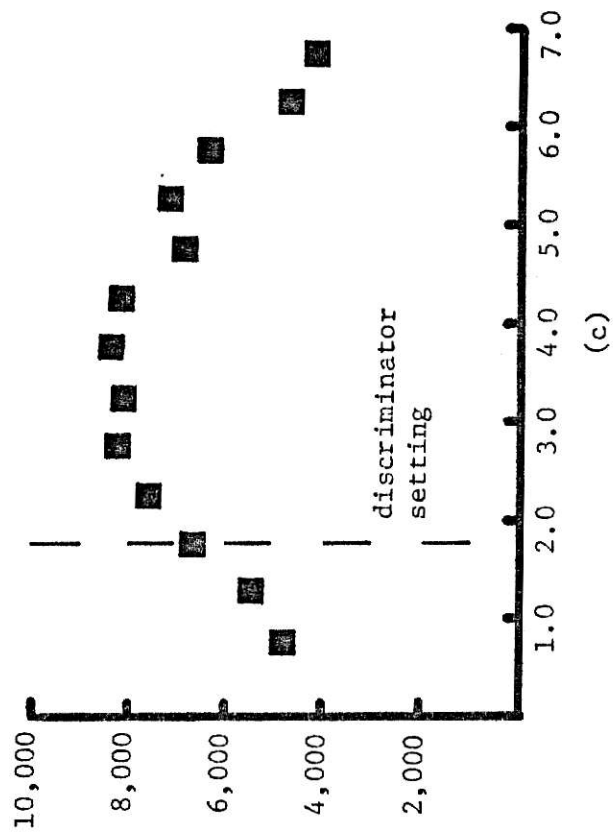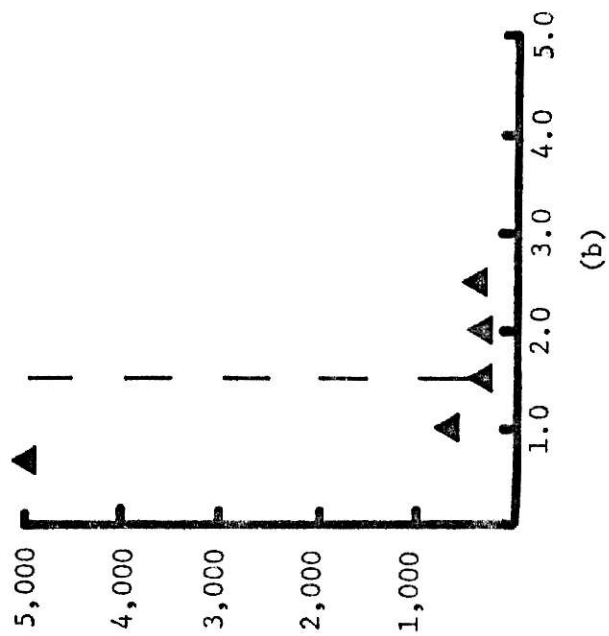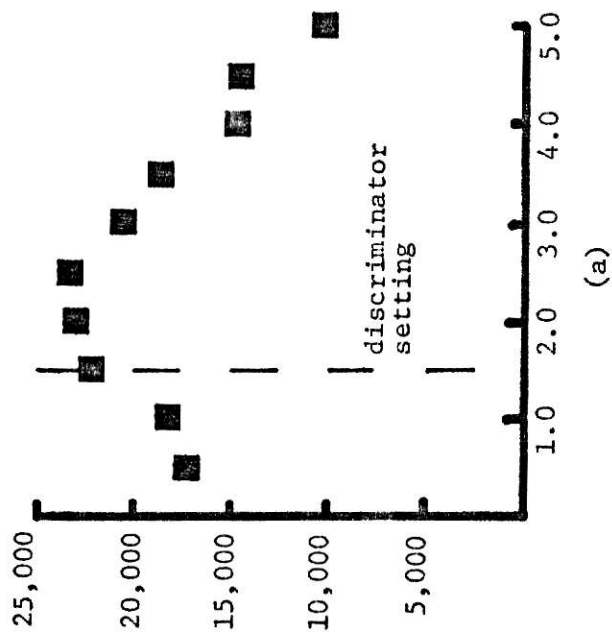
Since this noise was correlated with the laser pulse, the gated method was ineffective against it. Only by careful shielding was it possible to reduce this correlated laser noise to a level that could be discriminated reliably without rejecting a large proportion of single photon events.

All experiments were performed on slices from single crystal Cu_2O boules grown by Brower and Parker[26] using a floating zone technique. The sample was mounted in a brass cell (see Fig. 10) using a low temperature varnish. Helium was used as an exchange gas to help prevent sample heating. An Air Products and Chemicals cryostat was used to cool the sample to 20K. Hydrogen gas was precooled below its inversion temperature by a liquid nitrogen bath and then liquified by the Joule-Thomson process. The back pressure above the liquid hydrogen could be adjusted to vary the bath temperature. A radiation shield enclosing the sample cell and a vacuum of less than 10^{-7} mm of Hg minimized heat losses. The sample temperature was monitored by a Chromel vs. Constantan thermocouple and a .07% iron doped gold vs. copper thermocouple.

The incident beam struck the sample at 60° off the normal. Appendix I contains the calculations for the reflectance at this angle of incidence. A small incident angle from the normal is better from the standpoint of producing a sharp line on the sample with minimal reflectance. However, it has its disadvantages in that the light scattered off the surface may not be able to completely exit the cell and so gives rise to an undesirable amount of scattered light being collected into the detector. Using an angle of 60° was convenient because of the construction of the sample cell. It also allowed most of the scattered light to leave the cell as well as enabling a sharp line to be focussed on the sample surface. Laser powers were

measured with a Scientech disc calorimeter laser power meter. Specifications include a flat spectral response from 0.3 to 30 microns and a measurable power range of 1 milliwatt to 3 watts.

FIGURE 10

The sample was mounted in a brass sample cell filled

with one atmosphere of helium gas.

attaches to cryostat

entrance window

incident beam

Cu_2O

exit window

Indium seal

scattered light
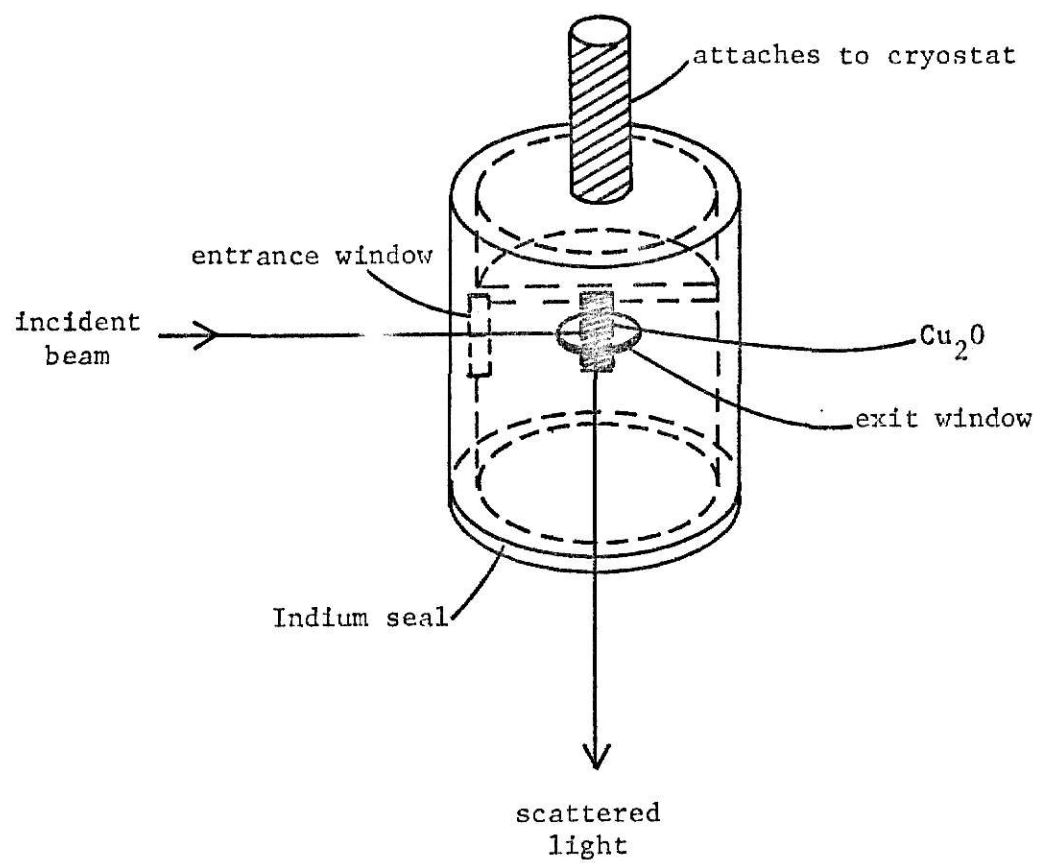
RESULTS AND ANALYSIS

CW Laser Experiments

Exciton luminescence spectra for four different CW laser excitation
frequencies can be seen in Fig. 11. The solid lines represent curve
fits using Eq. (4) and therefore determine characteristic exciton
temperatures, T^*. In each case the exciton system has not reached
equilibrium with the sample which is at 20K. This is an example of hot
exciton luminescence resulting from an exciton lifetime that is too short
to allow complete thermalization. When excitons are created near the
bottom of the band and therefore with kinetic energy that is close to
the lattice thermal energy, the final thermalization temperature depends
strongly on the pumping frequency. However when excitons are created
with kinetic energies in excess of ~ 100 cm^{-1}, the value of T^* has no
observable dependence on pumping frequency as seen in Figs. 11 and 12.
Although there is some variation in T^*, it is probably within the
uncertainties of the curve fits and the statistical fluctuations in the
data.

Since the exciton lifetime is one of the critical factors in the
study of exciton kinetics, it is worthwhile to attempt an estimate of
its value. Three experiments have been performed for this purpose
with the results being consistent and placing clear boundary limits on
this lifetime. The first involves a two-phonon resonant Raman experiment
similar to that reported by Yu, et al.[27] This experiment consists of
measuring the Raman cross section for the 220 cm^{-1} line in the region

FIGURE 11

Luminescence spectra for CW laser excitation of
different frequencies. A significant dependence
of the exciton temperature on laser frequency is
apparent for the lower frequencies. The two Γ_{12}^{-}
phonon Raman feature can be seen in the form of
one high point in some of the data.

$\omega_\ell = 16530 \text{ cm}^{-1}$
$T^* = 26K$

$\omega_\ell = 16555 \text{ cm}^{-1}$
$T^* = 35K$

$\omega_\ell = 16600 \text{ cm}^{-1}$
$T^* = 43K$

$\omega_\ell = 16800 \text{cm}^{-1}$
$T^* = 45K$

16400   16300

16400   16300

Frequency (cm^{-1})

45
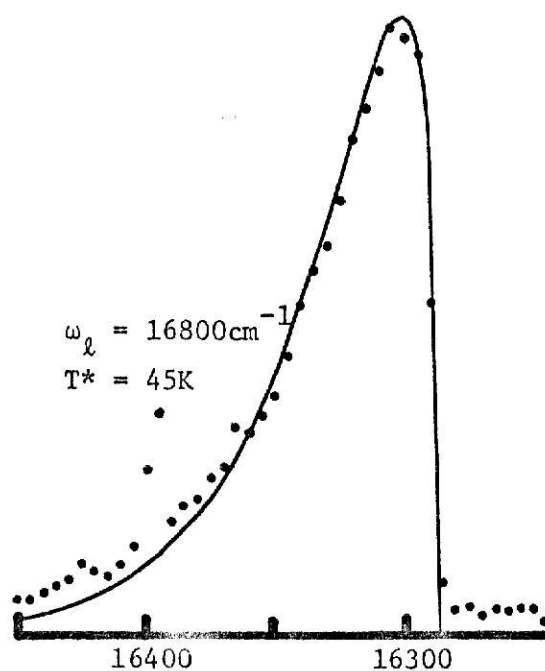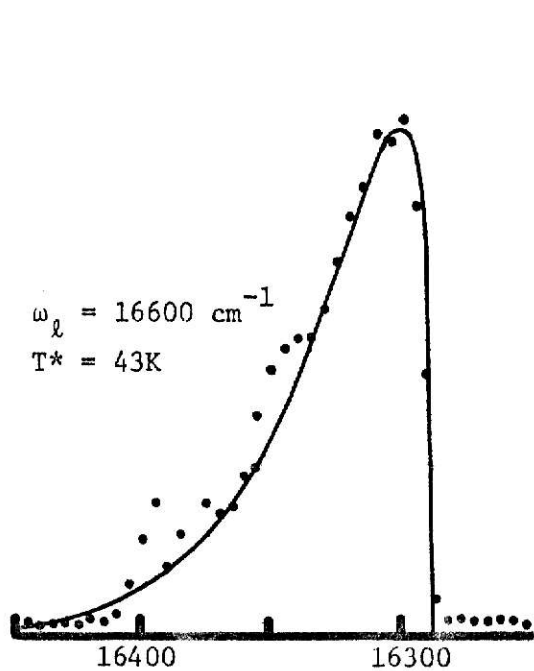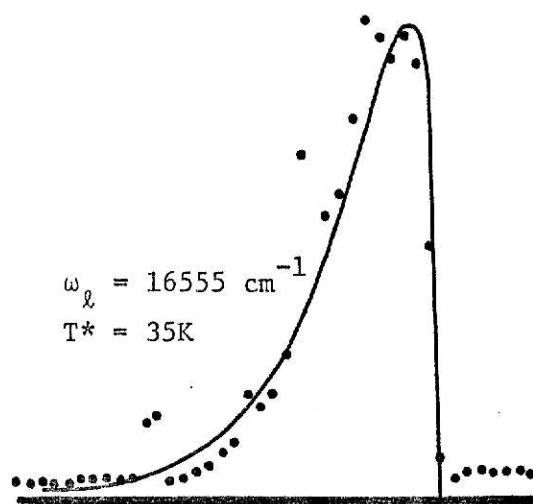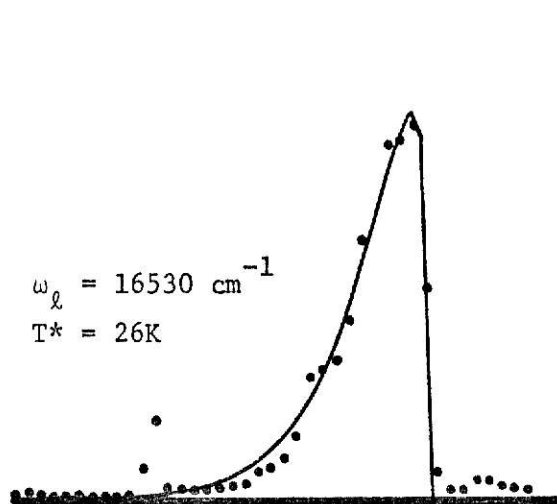
FIGURE 12

Luminescence spectra for CW laser excitation of
different frequencies. There appears to be no
exciton temperature dependence on laser frequencies
in this range.

$\omega_\ell = 16700 \text{ cm}^{-1}$

$T^* = 42K$

$\omega_\ell = 16750 \text{ cm}^{-1}$

$T^* = 43K$

$\omega_\ell = 16900 \text{ cm}^{-1}$

$T^* = 40K$

$\omega_\ell = 17255 \text{ cm}^{-1}$

$T^* = 43K$

16400   16300

16400   16300

Frequency (cm^{-1})

47
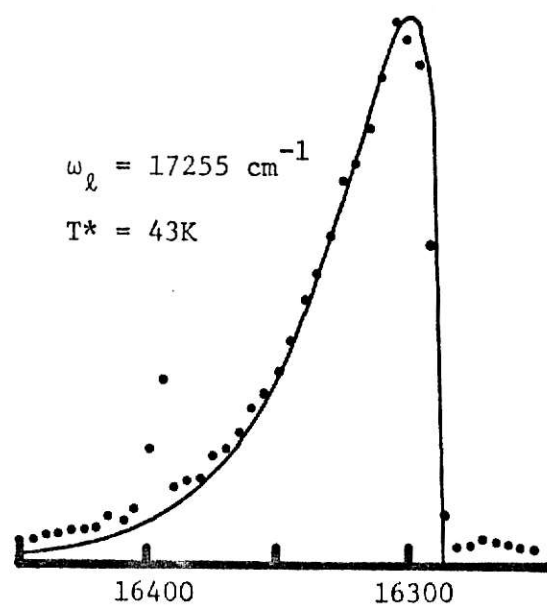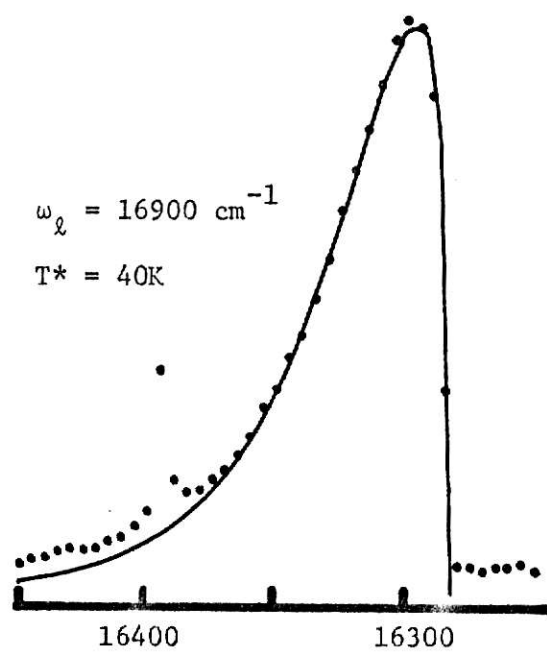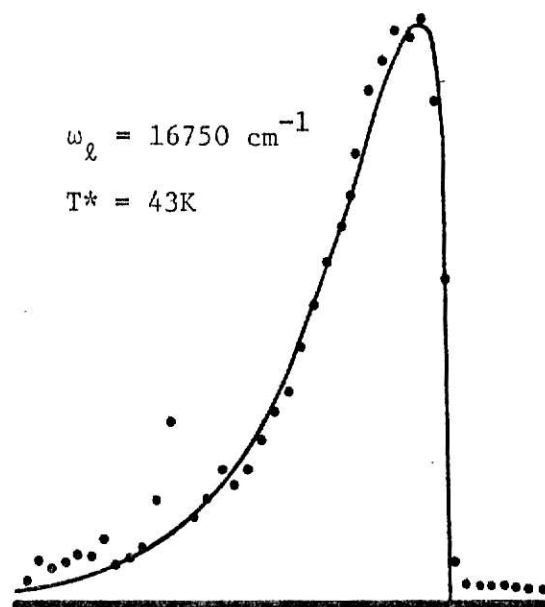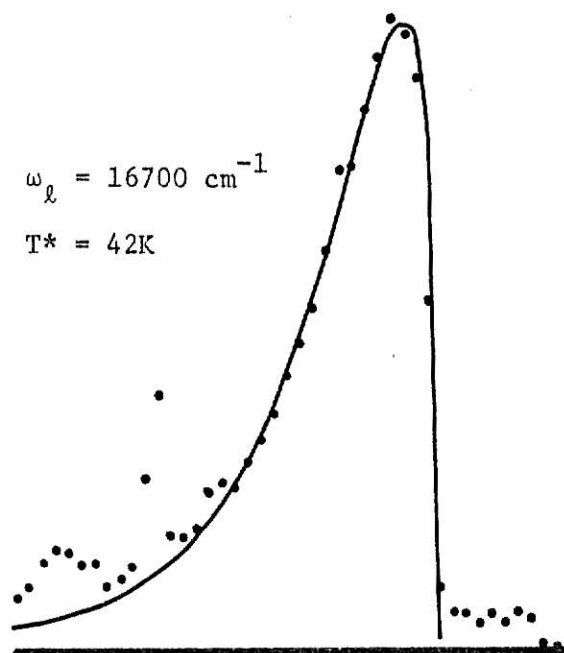
of the phonon-assisted yellow exciton absorption band. The 220 cm^{-1} line can be attributed to scattering by two Γ_{12}^- phonons. The enhancement results from resonance with an intermediate exciton state of the 1S yellow exciton. The incident photon is absorbed creating a Γ_{12}^- phonon and an exciton. The exciton then decays emitting another Γ_{12}^- phonon and a photon. The emitted photon is therefore shifted two Γ_{12}^- phonon frequencies (218 cm^{-1}) from the incident photon. Any process that removes the intermediate exciton from its initial state by other than Γ_{12}^- phonon-assisted radiative decay, reduces the strength of the 220 cm^{-1} feature. Therefore a study of the Raman cross section provides information concerning the lifetime of the resonant state. Because the results of the experiment depend upon the sample used and on the temperature, the experiment of Yu and Shen has been repeated at 20K with the same sample used for all other experiments presented in this thesis.

The lifetime dependence of the Raman intensity can be expressed as the ratio of the total exciton lifetime to the radiative decay lifetime. One would also expect the intensity to be proportional to the absorption of the exciting light so that to a good approximation[28]

$$R(\bar{v}_i) \propto \frac{[\bar{v}_i - \bar{v}_1 - \bar{v}_o]^{1/2}}{\gamma(\bar{v}_i - \bar{v}_1 - \bar{v}_o)}$$

The numerator expresses the density of exciton states dependence for the absorption and $\hbar/\gamma(\bar{v}_i - \bar{v}_1 - \bar{v}_o)$ is the total exciton lifetime at the position $(\bar{v}_i - \bar{v}_1 - \bar{v}_o)$ on the band. The lifetime is determined by a variety of processes with scattering by two Γ_{12}^- phonons, scattering by

acoustic phonons, and nonradiative decay being the most dominant. The scattering by two Γ_{12}^- optic phonons can be eliminated by considering only the range of incident energies $\bar{\nu}_i < \bar{\nu}_1 + 3\bar{\nu}_o$. To a good approximation it is therefore possible to write $\gamma = \gamma_{ac} + \gamma_{n.r.}$ for $\bar{\nu}_1 + \bar{\nu}_o < \bar{\nu}_i < \bar{\nu}_1 + 3\bar{\nu}_o$ with γ_{ac} being the acoustic phonon scattering contribution and $\gamma_{n.r.}$ the nonradiative decay contribution. In 1958 Toyozawa published a general theory for the line shapes of exciton absorption bands.[29] His analysis of exciton-phonon interactions results in the following expression for exciton-acoustic phonon scattering

$$\gamma_{ac} = \left[\frac{4m^*V_o k_B (C_v - C_c)^2 2w_{ac}}{9\pi\hbar^3 Mu^2}\right]T \qquad \begin{array}{l} \text{Region I} \\ K_{ex} < w_{ac} \end{array}$$

$$= \left[\frac{4m^*V_o k_B (C_v - C_c)^2}{9\pi\hbar^3 Mu^2}\right]\left[\frac{K_{ex}^2 + w_{ac}^2}{K_{ex}}\right] \begin{array}{l} \text{Region II} \\ K_{ex} > w_{ac} \end{array}$$

where $w_{ac} = m^*u/\hbar$ and T is the lattice temperature. V_o and M are the volume and mass of the unit cell while u is the average velocity of sound in the crystal. C involves the deformation potential of the energy band or the kinetic energy of the Bloch function depending upon the approximation model used in describing the acoustic mode of vibration. The expression for Region I is applicable for excitons with essentially zero momentum and therefore can be applied to the experimental results obtained by Merle, et al.[30] for the temperature dependence of the n = 1 line shape.

$$\gamma_{ac} = (12 \times 10^{-3} \text{ cm}^{-1}/K)T \qquad \text{Region I}$$

This result can be used to determine the constant of proportionality between γ_{ac} and T in Toyozawa's expression and can then be applied to Region II.

$$\gamma_{ac} = (12 \times 10^{-3} \text{ cm}^{-1}/\text{K}) \left[\frac{K_{ex}^2 + w_{ac}^2}{2 w_{ac} K_{ex}} \right] T \tag{5}$$

For low temperatures $(T \ll \Theta)$ T must be replaced by

$$\Theta = \frac{2\hbar u}{3 k_B} \frac{(K_{ex} + w_{ac})^3}{(K_{ex}^2 + w_{ac}^2)}$$

so that Eq. (5) becomes

$$\gamma_{ac} = \frac{(12 \times 10^{-3} \text{ cm}^{-1}/\text{K})}{2 w_{ac} K_{ex}} \frac{(K_{ex} + w_{ac})^3}{2 w_{ac} K_{ex}} \frac{2\hbar u}{3 k_B} \quad .$$

Over a major part of the range of photon energies $(\bar{\nu}_1 + \bar{\nu}_o < \bar{\nu}_i < \bar{\nu}_1 + 3\bar{\nu}_o)$ it is a good approximation to assume $K_{ex} \gg w_{ac}$ so that

$$\gamma_{ac} = (12 \times 10^{-3} \text{ cm}^{-1}/\text{K}) \left[\frac{2\hbar u}{3 k_B} \right] \left[\frac{k_{ex}^2}{2 w_{ac}} \right] \quad . \tag{6}$$

The bottom of the exciton band is at $E_o = hc\bar{\nu}_1$ so that by Eq. (2)

$$K_{ex}^2 \propto (\bar{\nu}_i - \bar{\nu}_1 - \bar{\nu}_o)$$

which means that

$$\gamma_{ac} \sim A[\bar{\nu}_i - \bar{\nu}_1 - \bar{\nu}_o] \quad . \tag{7}$$

50

Therefore, the Raman cross section can be written as

$$R(\bar{\nu}_i) \propto \frac{[\bar{\nu}_i - \bar{\nu}_1 - \bar{\nu}_o]^{1/2}}{A[\bar{\nu}_i - \bar{\nu}_1 - \bar{\nu}_o] + \gamma_{n.r.}}$$

$$\propto \frac{[\bar{\nu}_i - \bar{\nu}_1 - \bar{\nu}_o]^{1/2}}{[\bar{\nu}_i - \bar{\nu}_1 - \bar{\nu}_o] + \gamma_{n.r.}/A}$$

$$\propto \frac{[\bar{\nu}_i - \bar{\nu}_1 - \bar{\nu}_o]}{[\bar{\nu}_i - \bar{\nu}_1 - \bar{\nu}_o] + C} \quad . \tag{8}$$

This is just the result arrived at by Yu, et al. In order to use this expression in fitting the Raman intensity, it was necessary to normalize the raw data to the incident laser power and correct for absorption of both the incident light and the scattered light. A discussion of the absorption correction is given in Appendix II. Applying a two parameter fit to the corrected data using Eq. (8), it is possible to determine a value for C. Figure 13 shows the results of a best fit using $C = 12 \text{ cm}^{-1}$. By choosing a value of $\bar{\nu}_i$ so that the conditions $K_{ex} \gg w_{ac}$ and $\bar{\nu}_i + \bar{\nu}_o < \bar{\nu}_i < \bar{\nu}_1 + 3\bar{\nu}_o$ are fulfilled, it is possible to determine the constant A from Eqs. (6) and (7) and thereby extract a value for $\gamma_{n.r.} = (A)(C)$. The result is a nonradiative decay lifetime of $\tau_{n.r.} = \hbar/\gamma_{n.r.} \sim 4 \times 10^{-11}$ seconds. This result assumes a nonradiative decay rate that is independent of exciton momentum. This is probably a reasonable assumption for this particular calculation although increased mobility could lead to a decreased lifetime in a more careful analysis.

FIGURE 13

Raman cross section of the 220 cm^{-1} line of Cu_2O
at 20K. The solid line is a curve fit using
Eq. (8) with the value $C = 12$ cm^{-1}.

53
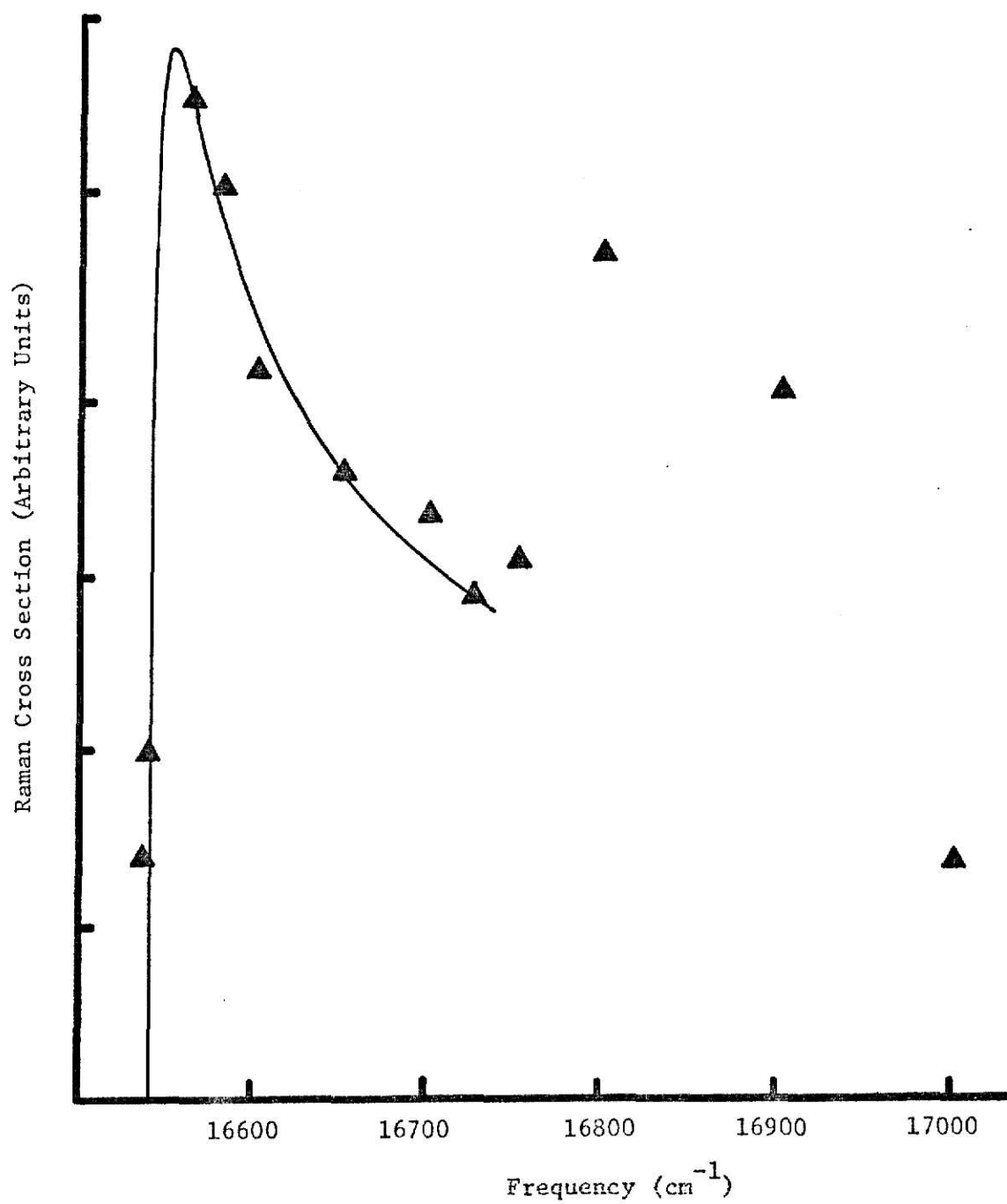
Two other experiments were performed in an attempt to determine the exciton lifetime by independent methods. A Time-to-Amplitude Converter (TAC) was used with a multichannel analyzer but the inherent width of the exciting laser pulse (7 nanoseconds) prevented a lifetime determination. The luminescence width was indistinguishable from the laser pulse width. This suggests a value of less than $\sim 1 \times 10^{-9}$ seconds. The final lifetime experiment involved a measurement of the width of the zero-phonon exciton recombination line. The full width was found to be ~ 0.3 cm^{-1} which indicates a decay lifetime that must be greater than $\sim 2 \times 10^{-11}$ seconds. Therefore the results of the three experiments seem to indicate an exciton lifetime that is roughly on the order of 1×10^{-10} seconds. Each experiment has important limitations. The Raman experiment was difficult to perform due to laser instability at the red end of the tuning range. Also, the results are very sensitive to the nature of the absorption correction applied. There are two data points that deviate considerably from the rest of the data which is a cause of concern. The linewidth measurement could only set a lower limit on the lifetime since there could be other contributions to the broadening. Of course the limitation of the TAC measurement was the laser pulse width.

Although the complete thermalization time must be longer than the exciton lifetime, its actual value is uncertain. In his recent review article, Permogorov[15] proposes a typical thermalization time in semi-conductors on the order of 10^{-10} to 10^{-9} seconds which is reasonably consistent with the above exciton lifetime. For higher sample temperatures, the degree of thermalization achieved should increase. This is due mostly to an increase in the exciton-phonon scattering rate further up

the band and the larger population of phonons. Data has also been taken for a sample temperature of 77K. The resulting exciton temperature was 88K. This data can be seen in Fig. 15a and will be discussed later. Although the exciton temperature was still higher than the sample temperature, the difference between the exciton and phonon temperatures was less as expected.

To further appreciate the degree to which complete thermalization has occurred, consider again the process by which an exciton system attempts to reach equilibrium with the lattice. When the excitons are far up on the band they lose their excess energy to the lattice by emitting phonons. As they near the lattice thermal energy there begins to be the possibility of absorbing phonons and the rate at which energy is transferred from the exciton system to the lattice decreases. As pointed out by Permogorov, complete equilibrium with the phonons can only occur after many interactions, including both absorption and emission. Using Eq. (6) it is possible to calculate an exciton-acoustic phonon scattering lifetime at a position on the band corresponding to a thermal energy for 45K. The result is $\hbar/\gamma_{ac} \sim 8\times10^{-12}$ seconds and suggests that many more than ten interactions with acoustic phonons are required by an exciton in order to equilibrate with the lattice during a 1×10^{-10} second exciton lifetime.

High Power Pulsed Laser Experiments

So far the results presented involved only a low density exciton system created by the CW laser. Figure 14 shows the luminescence spectra

FIGURE 14

Luminescence from pulsed laser excitation at
17000 cm^{-1} and different power densities.

Luminescence (cts/40 sec) vs. Frequency (cm⁻¹) spectra at four excitation powers:

(a) P = 4.7 W/cm², T* = 40K

(b) P = 6.7 MW/cm², T* = 45K, ×10

(c) P = 11 MW/cm², T* = 55K, ×10

(d) P = 22 MW/cm², T* = 65K, ×14.3

Vertical axis: LUMINESCENCE (cts/40 sec)
Horizontal axis: FREQUENCY (cm⁻¹), 16 500 — 16 400 — 16 300
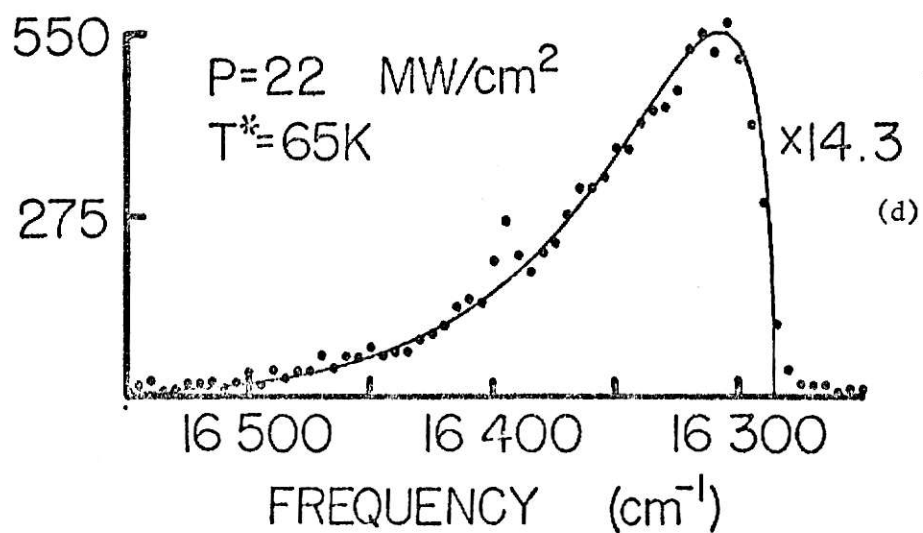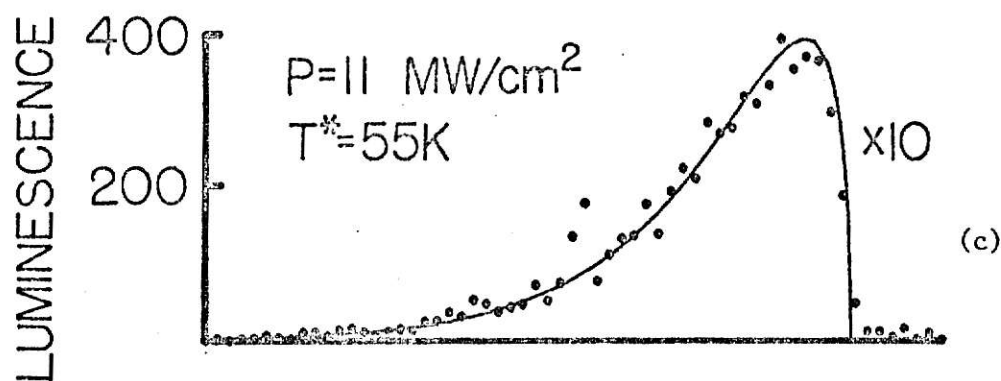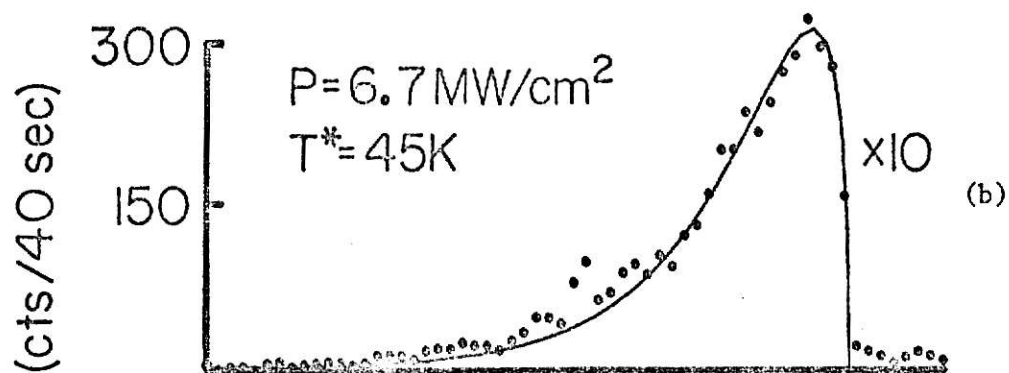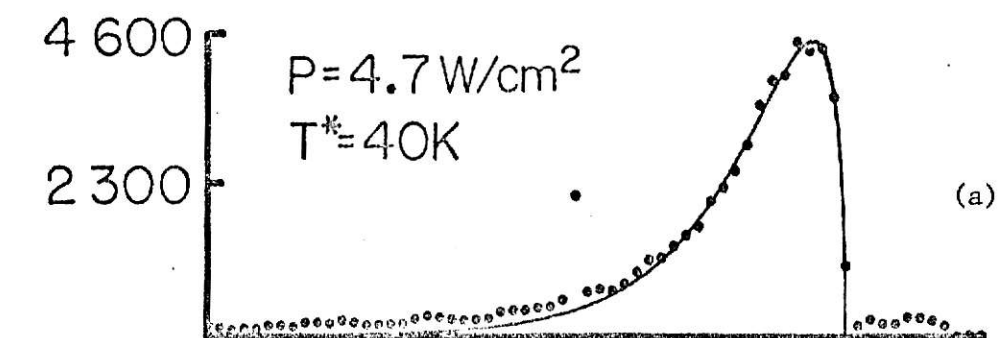
obtained for a variety of laser power densities all with a pumping frequency of 17000 cm^{-1}. Excitons are therefore created with 496 cm^{-1} of kinetic energy which is still 429 cm^{-1} below the bottom of the n = 2 yellow exciton band and 629 cm^{-1} from the continuum. It is clear that the effective exciton temperature depends rather strongly on the laser intensity. Factors that could account or contribute to this temperature dependence are: 1) a decrease in the exciton lifetime, 2) an increase in the optic and/or acoustic phonon populations or temperatures, 3) an increase in the number of exciton-exciton collisions. In the arguments that follow it will be shown that number three offers the most feasible explanation.

Any process that shortens the exciton lifetime would lead to a luminescence sideband that is broadened as discussed earlier for low power studies. It would not be reasonable to suspect that high exciton densities could lead to inelastic collisions which would shorten the lifetime of the free exciton. These processes would give rise to additional nonradiative decay and to radiative decay in other spectral regions, thus there would be a decrease in the luminescence quantum efficiency. Upon integrating the area under the sidebands of figures 14a, 14b, 14c, and 14d and normalizing the results to the number of incident photons, it was found that the quantum efficiencies were essentially the same and independent of incident power. Therefore a shorter exciton lifetime does not seem to be an adequate explanation.

Since both the absorption and luminescence processes are phonon-assisted, one might expect a Γ_{12}^- optic phonon population which is higher than the population consistent with a lattice temperature of 20K. In addition, exciton relaxation by the emission of two Γ_{12}^- phonons is

a dominant process for excitons with over 220 cm^{-1} of kinetic energy.
As reported by Meneses, et al.,[24] a nonequilibrium distribution of optic
phonons caused by intense laser excitation can cause broadening in
emission spectra of semiconductors. It is possible to at least put an
upper limit on the population of this optic phonon by considering the
anti-Stokes luminescence process. The probability of an anti-Stokes
transition, involving the decay of an exciton into a photon accompanied
by the absorption of a phonon, is proportional to the same matrix element
and the same density of final states as the Stokes process. However,
the Stokes transition is proportional to the occupation number of the
phonons plus one (n+1) while the anti-Stokes is proportional to n.
Therefore the ratio of the two types of emission should be

$$\frac{I_{AS}}{I_S} = \frac{n}{n+1} = \exp(-hc\bar{\nu}_o/kT_o) \quad .$$

T_o describes the "temperature" of the optic phonon assisting in the
luminescence while $\bar{\nu}_o$ is the frequency of the phonon. The anti-Stokes
sideband is clearly seen in Fig. 15a. The curve fit corresponds to an
optic phonon temperature of 77K. A repetition of the spectrum from
Fig. 14d is shown in Fig. 15b with a curve fit for an optic phonon
temperature of 65K showing where the anti-Stokes edge would appear. By
checking the intensity ratio for nine points over the two bands, it is
possible to place an upper limit of $T_o \leq 40K$ for the 109 cm^{-1} phonon
temperature under the highest intensity excitation used. The details
of this analysis are contained in Appendix III. It is doubtful that
this would be a large enough increase to cause an exciton temperature of 65K.

(a)

(b)

61
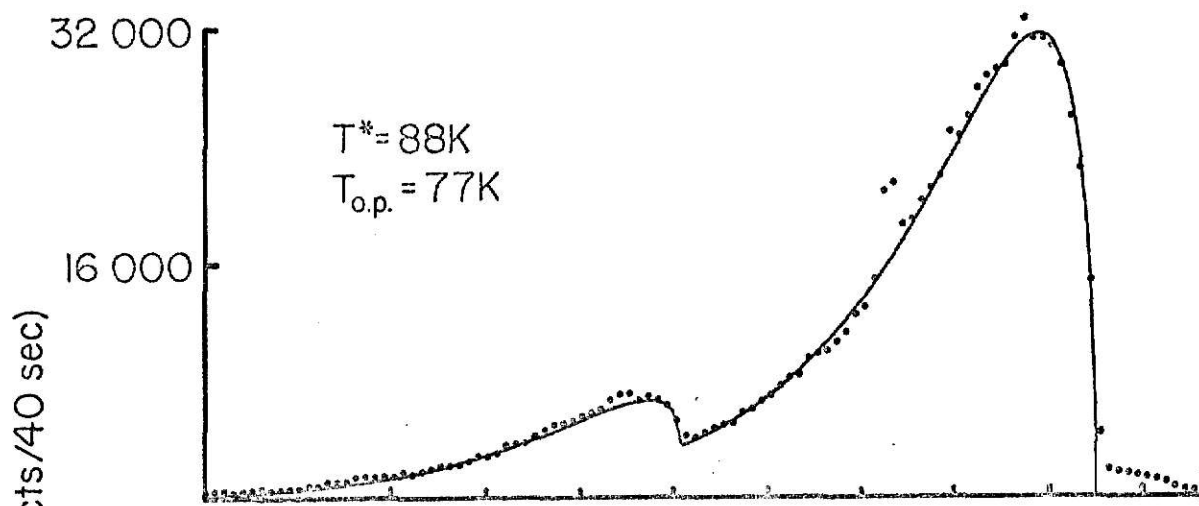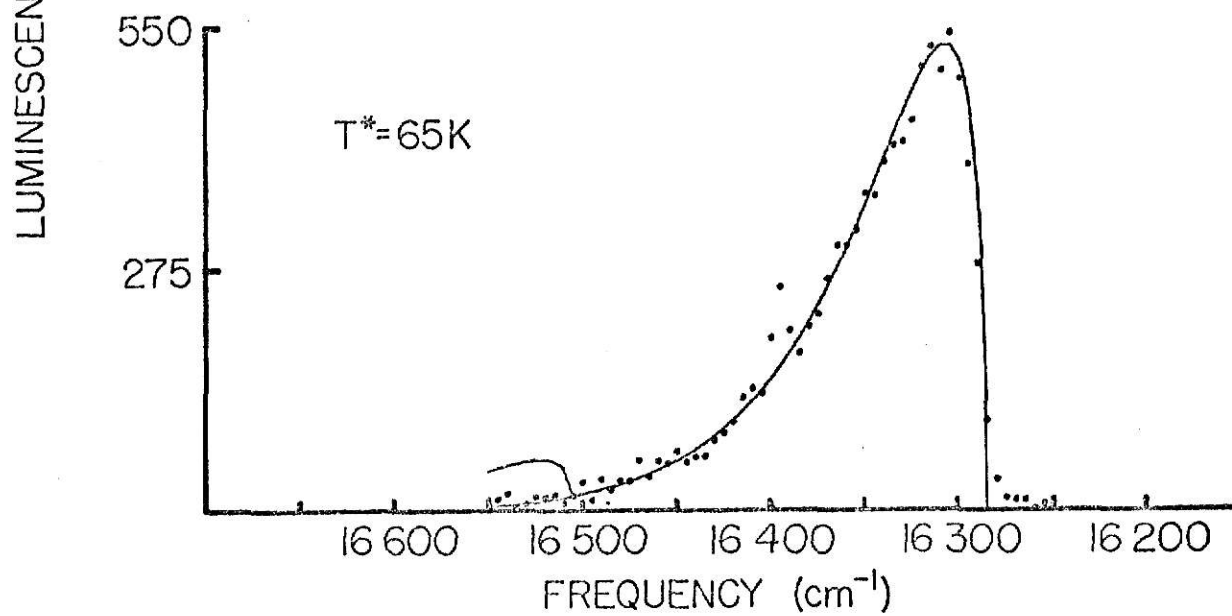
A large number of excess optic phonons are certainly created but they probably decay very rapidly into acoustic phonons. Using the 220 cm^{-1} Raman line, the Γ_{12}^{-} two optic phonon linewidth was determined to be .75 cm^{-1} so that the decay lifetime of the phonon is approximately 1×10^{-11} seconds. Since the laser pulse is 7 nanoseconds, this lifetime could certainly be short enough to warrant concern about the acoustic phonon population.

Any long term heating effects on acoustic phonons can be ruled out since this would result in a shift in the position of the sideband edge. Figure 15 shows this shift in the two sets of data taken with bath temperatures of 77K and 20K. A more precise indication of the shift with lattice temperature is given in Fig. 16. The temperature was monitored by a thermocouple while changing the hydrogen back pressure on the cryostat. The shift in the position of the zero-phonon line is due to the temperature dependence of the band gap and is in good agreement with the results of Nikitine, et al.[31] Since the positions of the zero-phonon lines for the different powers are the same to within 5 cm^{-1}, any long term (over several pulses) temperature changes were less than 8K and therefore not likely responsible for the observed broadening. However, changes in the acoustic phonon populations on a nanosecond time scale might not be reflected in a shift of the sideband. Again it is possible to place an upper limit on the acoustic phonon temperature rise after a laser pulse by using a Debye specific heat calculation. If C_v is the specific heat capacity and ΔE is the amount of excess energy deposited in the excited region of the crystal by one laser pulse, then

$$\Delta E = \int_{20}^{T_f} C_v \, dT \quad .$$

62

FIGURE 16

Experimentally observed position of the zero-phonon

line for different lattice temperatures.

64
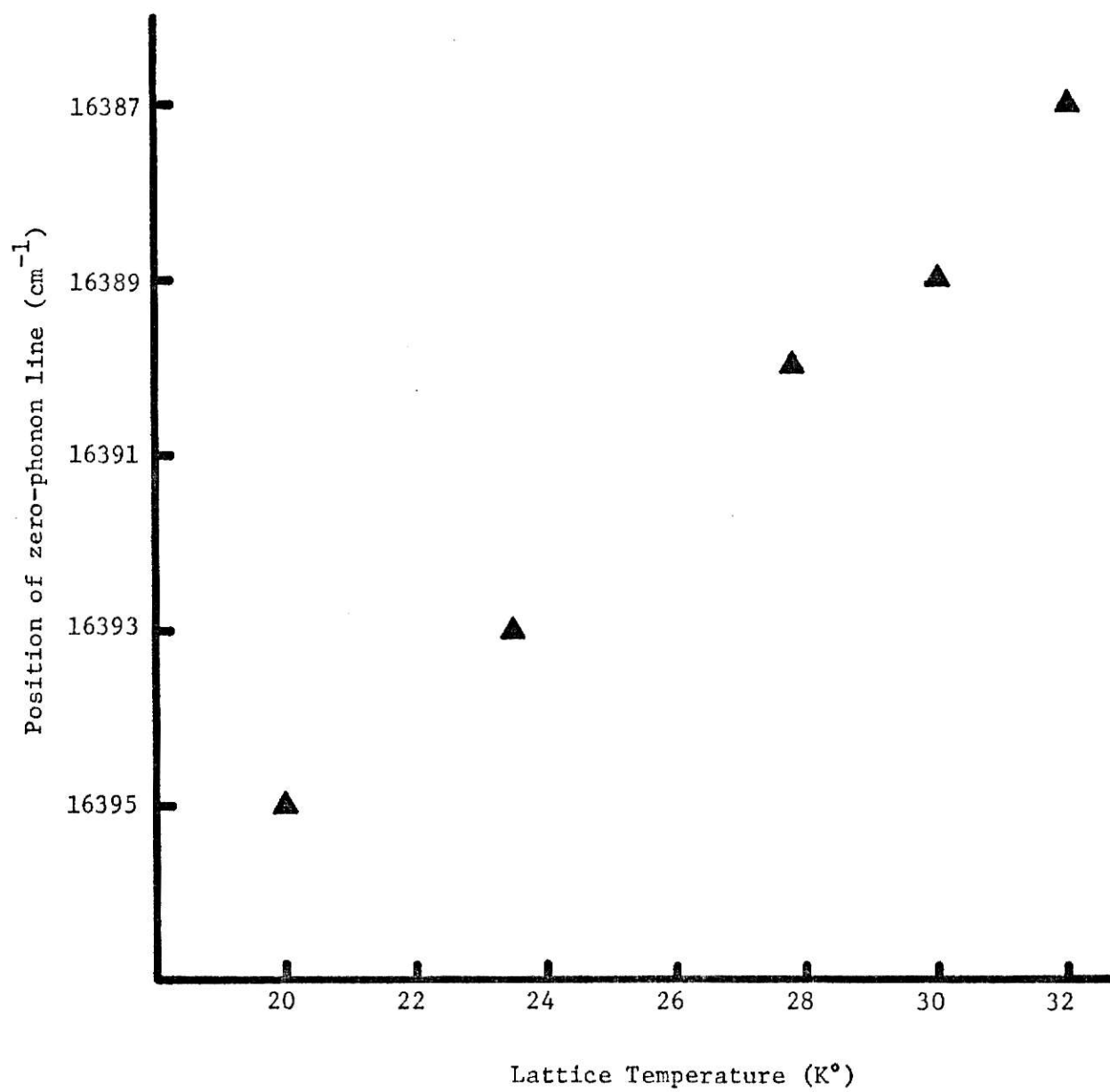
Applying the results of Appendix IV for the heat capacity yields

$$\Delta E = (2 \times 10^{-3} \ \text{erg/K}) \int_{20}^{T_f} T^3 \ dT$$

Performing the integration and solving for the final temperature resulting from one laser pulse results in

$$T_f = [(2 \times 10^3 \ \text{K}^4/\text{erg})\Delta E + (20\text{K})^4]^{1/4}$$

An estimate of ΔE can be made by considering the difference in the incident energy and the energy given up in luminescence. The two main luminescence features are the Γ_{12}^{-} phonon sideband and a broad impurity band which is shown in Fig. 17. Because the impurity band is so broad, it was necessary to correct the raw data for the spectral throughput of the spectrometer and photomultiplier tube. However, upon integrating the energy under these features, it was evident that they constituted an insignificant fraction of the incident energy. Using then the total energy delivered in one laser pulse as ΔE in the case of the highest power density used, results in an upper limit for the acoustic phonon temperature of

$$T_f = [(2 \times 10^3 \ \text{K}^4/\text{erg})(544 \ \text{ergs}) + (20\text{K})^4]^{1/4}$$
$$\sim 34\text{K}$$

This is well below the temperatures observed for the exciton system and therefore acoustic phonon heating is not likely responsible for the sideband broadening. This conclusion can be further supported by considering the exciton temperature dependence on the laser power. The

FIGURE 17

Cu_2O luminescence data corrected for spectrometer
throughput (see Fig. 6). The data was taken with
the CW laser at a frequency of 16950 cm^{-1}. The
bath temperature was 20K.
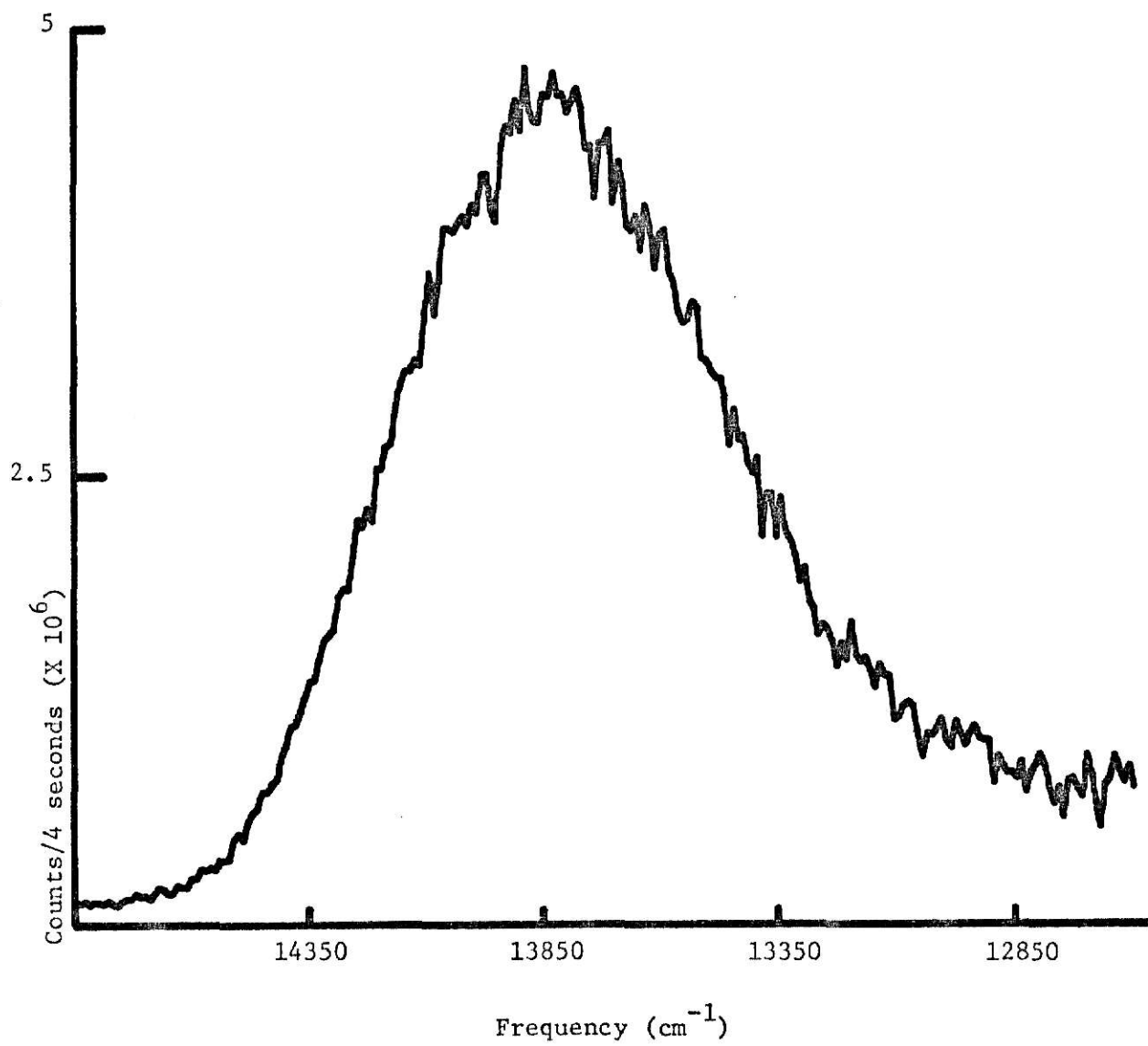
Debye theory indicates essentially a fourth root dependence on the laser power whereas the actual dependence is much stronger. This is shown in Fig. 18. It is therefore evident that neither shorter exciton lifetimes nor optic and acoustic phonon heating can be used to adequately explain the observed dependence of the effective exciton temperature on laser power density. In the discussion that follows, it will be shown that the observations can be understood on the basis of elastic exciton-exciton scattering.

If high density excitons are initially created with a large excess energy, they will scatter down the exciton band very quickly through phonon relaxations until they reach a point on the band where exciton-exciton scattering can compete with exciton-acoustic phonon scattering. The excitons are then able to exchange energy within the exciton system and effectively "thermalize" to a higher effective temperature than they would in a low density system. If the exciton system is treated as a gas of hard spheres, it is possible to calculate a scattering lifetime based upon an estimated density and compare it with the acoustic phonon scattering lifetime at the point on the band representing kT* of energy.

For the highest power density case (Fig. 14d), the excitation frequency was 17000 cm^{-1} corresponding to an absorption constant of 87.7 cm^{-1}. Using the measured power density of 22.3 MWatts/cm^2, an absorptance of 0.78, and the estimated nonradiative lifetime of 10^{-10} seconds, the exciton density created was

$$\frac{\dot{N}}{V} = \frac{(22.3 \times 10^{13} \text{ ergs/cm}^2 \text{ sec})(87.7 \text{ cm}^{-1})(.78)(10^{-10} \text{ sec})}{hc(17000 \text{ cm}^{-1})}$$

$$\sim 4.5 \times 10^{17} \text{ cm}^{-3} \quad .$$

FIGURE 18

T* and T_f are plotted against the total amount of

energy delivered to the sample per laser pulse. T*

was determined from curve fits using Eq. (4) while

T_f is calculated using the Debye model for the

specific heat.
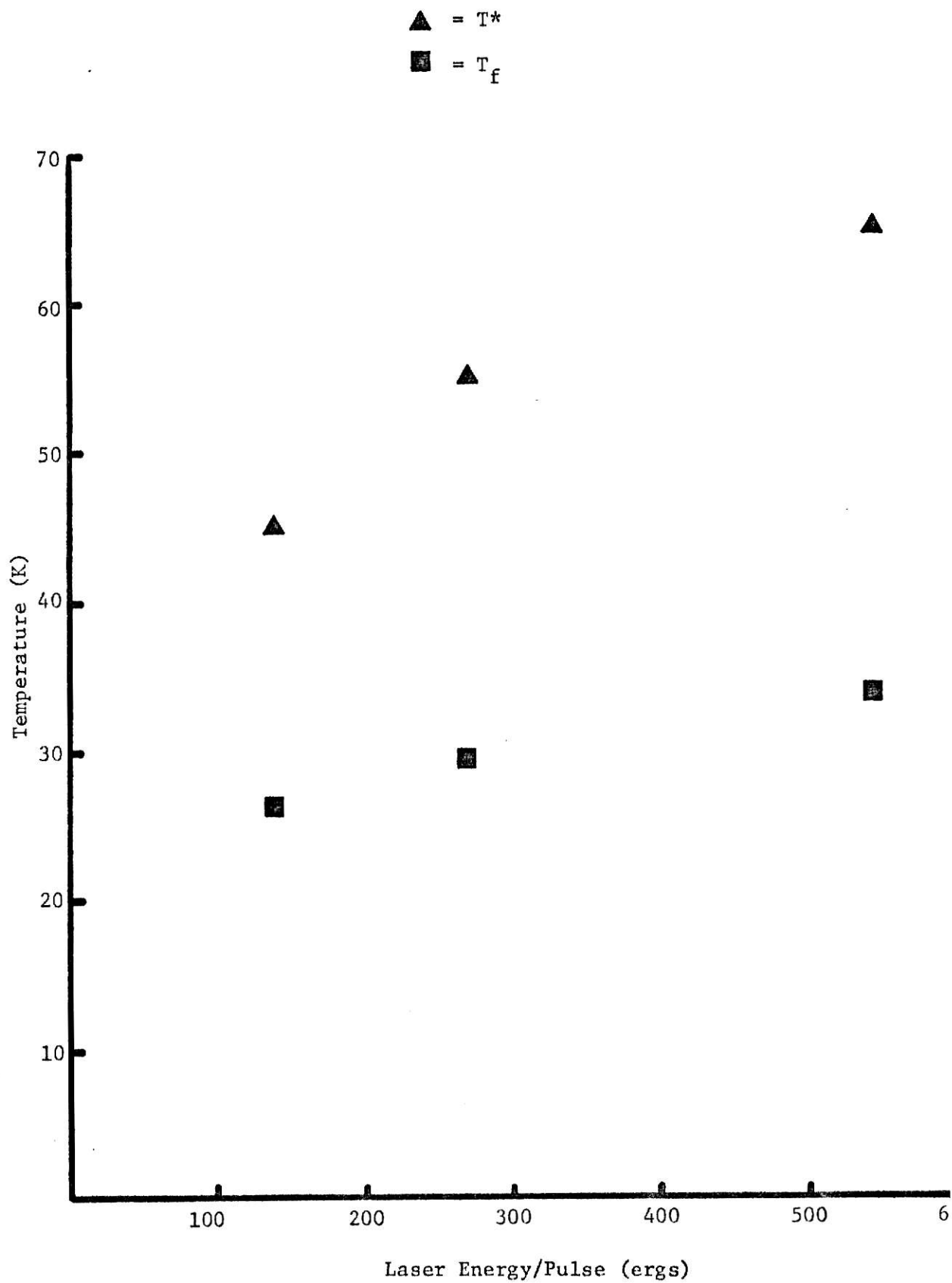
Using this density, a lifetime for exciton-exciton scattering can then be determined.

$$\tau^{-1}_{ex-ex} = \overline{V} \sigma_o \frac{N}{V}$$

$$= \sqrt{2} \; \overline{V} \sigma_o \frac{N}{V}$$

$$= \sqrt{2} \; \sqrt{\frac{8kT^*}{\pi m^*}} \; \sigma_o \frac{N}{V}$$

$$= 4 \sqrt{\frac{kT^*}{m^*}} \; \pi (2r_{ex})^2 \frac{N}{V}$$

$$= 4\pi (2r_{ex})^2 \frac{N}{V} \sqrt{\frac{kT^*}{\pi m^*}}$$

Substituting $r_{ex} = 7 \times 10^{-8}$ cm, $T^* = 65K$, and $m^* = 3m_o$ results in a lifetime of $\tau_{ex-ex} \sim 1 \times 10^{-11}$ seconds. This compares to an exciton acoustic phonon scattering lifetime of 6×10^{-12} seconds at kT^* on the band which can be obtained from Eq. (6).

These results support the view that for excitons created in sufficient density, exciton-exciton collisions are responsible for a "hot" exciton system whose effective temperature is considerably higher than that for a low density system. The relatively strong dependence of the exciton temperature on laser power density is consistent with the exciton-exciton scattering rate's linear dependence on exciton density. The estimated exciton lifetime and exciton-acoustic phonon scattering rate also support this explanation. As the exciton density increases, the exciton-exciton

71

scattering rate approaches the exciton-acoustic phonon scattering rate
with both processes occurring many times during the exciton lifetime.

SUMMARY AND CONCLUSIONS

This thesis has reported the observation of hot exciton luminescence in Cu_2O resulting from a short free exciton lifetime. An estimate of that lifetime has been proposed which is consistent with the data. Effective temperatures of exciton systems under a variety of pumping frequencies and laser powers have been measured. A strong dependence of the exciton temperature on laser power density has been attributed to exciton-exciton scattering competing with exciton-acoustic phonon relaxation. The results of that analysis can be summarized for the highest laser intensity used:

$$\tau_{ex} \sim 1 \times 10^{-10} \text{ seconds}$$

$$\tau_{ex-ex} \sim 1 \times 10^{-11} \text{ seconds}$$

$$\tau_{ex-ac} \sim 6 \times 10^{-12} \text{ seconds}$$

There are many additional experiments that can be performed to shed further understanding on these results. For example, a direct lifetime measurement of the free exciton lifetime with a picosecond laser would be very helpful in determining more precisely this critical parameter. High density studies at liquid helium temperatures would test some of the above hypotheses by reducing phonon effects. A better theoretical understanding of exciton-phonon kinetics and the thermalization process would also be beneficial.

73

It is hoped that this thesis will provide the necessary foundation
for future studies of exciton-exciton and exciton-acoustic phonon inter-
actions in Cu_2O. Further, it is anticipated that these techniques will
find application to other direct gap semiconductors with similar properties.
It is also hoped that the experience gained in the experimental methods
related to this type of study will be beneficial in the understanding of
future experiments.

Appendix I

Calculation of Absorptance and Reflectance

The incident laser beam makes an angle of 60° from the normal to the face of the sample. Therefore from Snell's Law, the angle of transmission is given by

$$\frac{\sin\Theta_t}{\sin\Theta_i} = \frac{n_1}{n_2} = \frac{1}{2.5}$$

$$\sin\Theta_t = \frac{\sin(60°)}{2.5}$$

$$\Theta_t = 20.3°$$

where 2.5 was used as the index of refraction for Cu_2O. From Fresnel's equations

$$[\frac{E_r}{E_i}]_N = \frac{[\frac{n_1}{n_2}] \cos(\Theta_i) - \cos(\Theta_t)}{[\frac{n_1}{n_2}] \cos(\Theta_i) + \cos(\Theta_t)}$$

$$= \frac{[\frac{1}{2.5}] \cos(60°) - \cos(20.3°)}{[\frac{1}{2.5}] \cos(60°) + \cos(20.3°)}$$

$$= -0.65$$

and

$$\left[\frac{E_r}{E_i}\right]_P = \frac{-\cos(\Theta_i) + [\frac{n_1}{n_2}]\cos(\Theta_t)}{\cos(\Theta_i) + [\frac{n_1}{n_2}]\cos(\Theta_t)}$$

$$\left[\frac{E_r}{E_i}\right]_P = \frac{-\cos(60°) + \frac{1}{2.5}\cos(20.3°)}{\cos(60°) + \frac{1}{2.5}\cos(20.3°)}$$

$$= 0.14 \quad .$$

For unpolarized light

$$(E_i)_N = (E_i)_P$$

and

$$(E_i)_N^2 + (E_i)_P^2 = (E_i)^2$$

so that

$$(E_i)_P = (E_i)_N = \frac{E_i}{\sqrt{2}} \quad .$$

Then from the relationship between E_i and E_r

$$(E_r)_N = \frac{(-.65)E_i}{2} \qquad \text{and} \qquad (E_r)_P = \frac{(.14)E_i}{\sqrt{2}}$$

76

so that

$$\frac{I_r}{I_i} = (\frac{E_r}{E_i})^2 = \frac{(-.65\ E_i)^2 + (.14\ E_i)^2}{2(E_i)^2}$$

$$= .22$$

Therefore the reflectance is 22% and the absorptance is 78% for the optical geometry of the experiments presented in this thesis.

Appendix II

Absorption Correction for Raman Scattering

The intensity of the Raman scattered light is proportional to the intensity of the incident laser beam at the point in the crystal where the light is scattered. This intensity will depend upon how much of the incident beam is absorbed in reaching that point. The actual intensity of the scattered beam will depend upon how much of it is absorbed as it leaves the scattering volume. Therefore an absorption correction must be applied to both beams.

Figure 19 shows the geometry of the incident and collected beams. Since the collected beam involves only a limited fraction of the total excited volume, a volume consideration must also be incorporated into the correction. If α_L and α_s are absorption constants for the laser and scattered beams, then the correction can be determined as follows.

$$dI_s(z) \propto I_L(z)\, e^{-\alpha_s z}\, w\, dz$$

$$\propto I_o\, e^{-\alpha_L z}\, e^{-\alpha_s z}\, w\, dz$$

$$\propto I_o\, e^{-(\alpha_L + \alpha_s)z}\, w\, dz$$

The determination of w is a matter of trigonometry with the result being

ILLEGIBLE DOCUMENT

THE FOLLOWING DOCUMENT(S) IS OF POOR LEGIBILITY IN THE ORIGINAL

THIS IS THE BEST COPY AVAILABLE

P-474

FIGURE 19

Diagram depicting the geometry involved in the

light scattering process. The index of refraction

for Cu_2O taken to be n = 2.5.
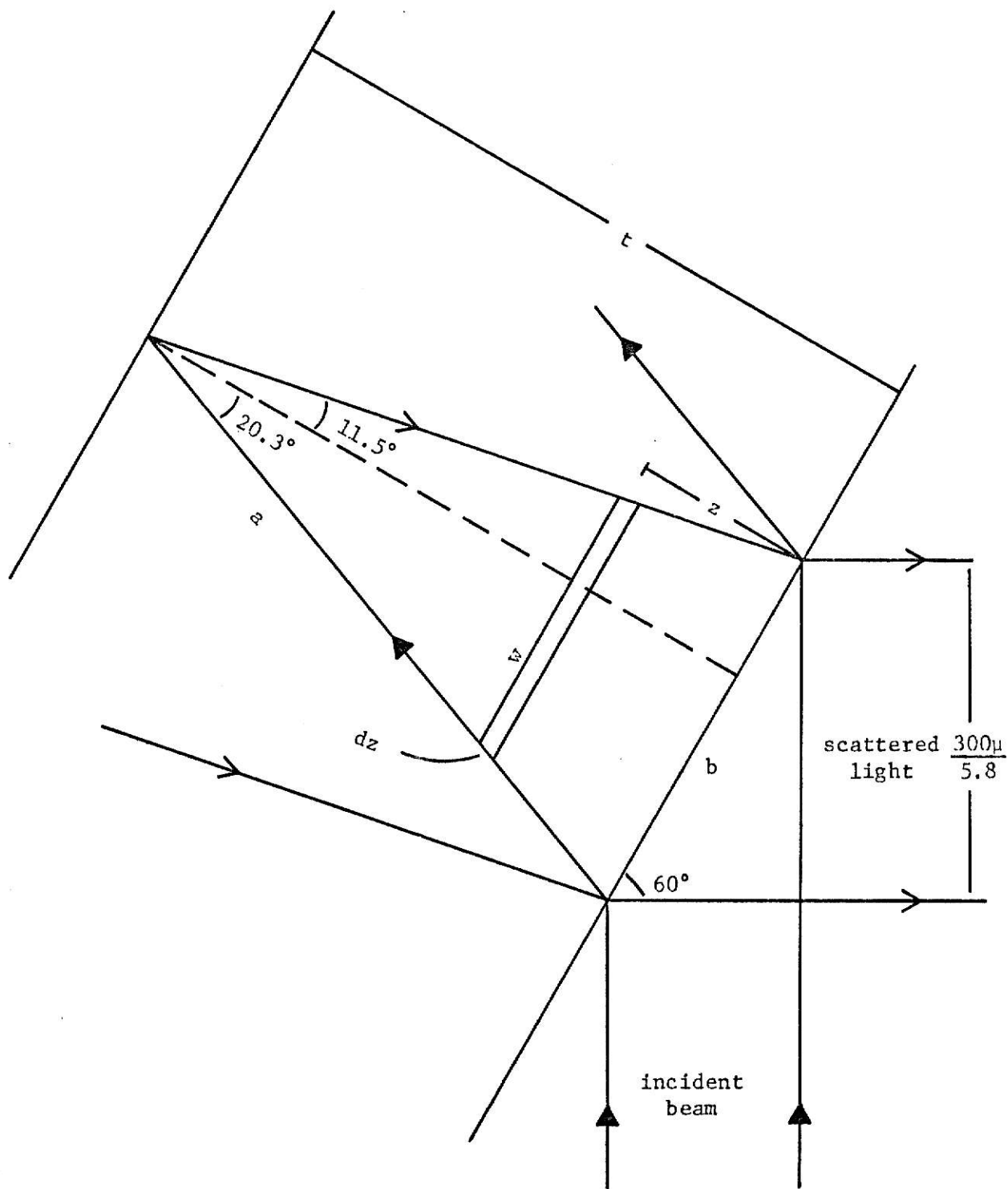
$$w = (t - z) \tan(11.5°) + (t - z) \tan(20.3°)$$

$$= (t - z)[\tan(11.5°) + \tan(20.3°)]$$

$$= (t - z) (0.57)$$

Therefore

$$I_s \propto \int_0^t (t - z) \, e^{-(\alpha_L + \alpha_s)z} \, dz$$

$$\frac{t}{(\alpha_L + \alpha_s)} - \frac{e^{-(\alpha_L + \alpha_s)t}}{(\alpha_L + \alpha_s)^2} + \frac{1}{(\alpha_L + \alpha_s)^2} \quad . \tag{9}$$

The value of t can be determined from the geometry of the problem.

$$t = a \sin(69.7)$$

$$= b[\frac{\sin(78.5)}{\sin(31.8)}] \sin(69.7)$$

$$= \frac{300\mu}{(5.8) \sin(60)} \frac{\sin(78.5)}{\sin(31.8)} \sin(69.7)$$

$$= 1.04 \times 10^{-2} \text{ cm}$$

Equation (9) can now be used to correct the Raman scattering data for absorption and collection volume.

Appendix III

Anti-Stokes to Stokes Ratio

As mentioned in the text, the anti-Stokes to Stokes ratio is a good way of determining the effective temperature of the phonon assisting in the luminescence process. The data which represents the largest phonon population for a bath temperature of 20K would be that of Fig. 14d. Therefore a study of this data will enable an upper limit to be placed on the Γ_{12}^- phonon population.

The Stokes intensity can be easily obtained by summing the area under nine points in the region of the sideband maximum. An estimate of the corresponding anti-Stokes intensity is obtained by summing the area under the companion points (220 cm^{-1} higher) in the region where the anti-Stokes peak would be. But one should consider only the area in excess of that due to the high energy tail of the Stokes luminescence. The magnitude of the tail is simply determined from Eq. (4). In addition, all points have been corrected for a dye fluorescence background that was estimated at 13 counts. The results are shown on the following page. Using those results, an optic phonon temperature can be determined.

$$\frac{58}{4118} = \exp\left[\frac{-hc(109 \text{ cm}^{-1})}{kT_o}\right]$$

$$\ln\left[\frac{58}{4118}\right] = \frac{-hc(109 \text{ cm}^{-1})}{kT_o}$$

$$T_o = 37K$$

Stokes Intensity

$\overline{v}(cm^{-1})$	Counts	Dye Background	Net Counts
16330	435	13	422
16325	459	13	446
16320	519	13	506
16315	541	13	528
16310	514	13	501
16305	557	13	544
16300	504	13	491
16295	409	13	396
16290	297	13	284
		TOTAL	4118

Anti-Stokes Intensity

$\overline{v}(cm^{-1})$	Counts	Stokes Backgnd.	Dye Backgnd.	Net Counts
16550	26	8	13	5
16545	34	9	13	12
16540	40	10	13	17
16535	24	11	13	0
16530	28	13	13	2
16525	37	14	13	10
16520	36	15	13	8
16515	39	17	13	9
16510	28	19	13	-5
			TOTAL	58

Appendix IV

Specific Heat Capacity for Cu_2O Using Debye Model

The Debye model for the lattice heat capacity is discussed in a variety of texts on thermodynamics and solid state physics[32] with the results being

$$C_v = 9NK_B[\frac{T}{\Theta}]^3 \int_o^{X_D} \frac{dx\ x^4 e^x}{(e^x-1)^2}$$

where $X = \frac{\hbar\omega}{KT}$ so that $X_D = \frac{\hbar\omega_D}{KT} = \frac{\Theta}{T}$. The Debye temperature has been reported by J. Hallberg[33] and R. C. Hanson as approximately 182K. If we consider only the number of atoms in the excited volume of the sample as contributing to the heat capacity, the result is

$$C_v = (9)(3.92\times10^{17})(1.38\times10^{-16}erg/K)\frac{T^3}{(182K)^3} \int_o^{\frac{182}{20}} \frac{dx\ x^4 e^x}{(e^x-1)^2}$$

Evaluating the integral numerically results in

$$C_v = (2.00\times10^{-3}erg/K)T^3 \quad .$$

REFERENCES

1. J. Frenkel, Phys. Rev. $\underline{37}$, 17 (1931); J. Frenkel, Phys. Rev. $\underline{37}$, 1276 (1931).

2. R. S. Knox, Theory of Excitons (Academic Press, New York, 1963).

3. M. Hayashi and K. Katzuki, J. Phys. Soc. Japan $\underline{5}$, 380 (1950); M. Hayaski, J. Fac. Sci. Hokkaido Univ. $\underline{4}$, 107 (1952).

4. E. F. Gross and N. A. Karryev, DAN SSSR $\underline{84}$, 261 (1952); E. F. Gross and N. A. Karryev, DAN SSSR $\underline{84}$, 471 (1952).

5. E. F. Gross, Advances in Phys. Sci. $\underline{63}$, 782 (1957).

6. E. F. Gross, Soviet Physics Uspekhi $\underline{5}$, 195 (1962).

7. S. Nikitine in Optical Properties of Solids, ed. by S. Nudelman and S. S. Mitra (Plenum Press, New York, 1969).

8. Excitons at High Densities, ed. by H. Haken and S. Nikitine (Springer-Verlag, New York, 1975).

9. J. P. Dahl and A. C. Switendick, J. Phys. Chem. Solids $\underline{27}$, 931 (1966).

10. R. J. Elliott, Phys. Rev. $\underline{124}$, 340 (1961).

11. E. F. Gross and B. P. Zakhartchornia, J. Phys. radium $\underline{18}$, 68 (1957); E. F. Gross and A. A. Kaplysnskii, Soviet Phys. - Solid State $\underline{2}$, 1518 (1961).

12. E. F. Gross, F. I. Kreingol'd, and V. L. Makarov, ZhETF Pis. Red. $\underline{15}$, 383 (1972).

13. P. Y. Yu and Y. R. Shen, Phys. Rev. Lett. $\underline{32}$, 939 (1974).

14. A. Compaan and H. Z. Cummins, Phys. Rev. B $\underline{6}$, 4753 (1972).

15. S. Permogorov, Phy. Stat. Sol. (b) $\underline{68}$, 9 (1975).

16. J. Shah, Phys. Rev. B $\underline{9}$, 562 (1974).

17. E. F. Gross, S. Permogorov, V. Travnikov, and A. Selkin, J. Phys. Chem. Solids $\underline{31}$, 2595 (1970).

18. E. F. Gross, S. Permogorov, Y. Morozenko, and B. Kharlamon, Phys. Stat. Sol. (b) $\underline{59}$, 551 (1973).

19. H. Kuroda, S. Shionoya, H. Saito, and E. Hanamura, Solid State Comm. $\underline{12}$, 533 (1973).

20. W. D. Johnston, Jr. and K. L. Shaklee, Solid State Comm. $\underline{15}$, 73 (1974).

21. W. Czaja and C. F. Schwerdtfeger, Solid State Comm. $\underline{15}$, 87 (1974).

22. H. Haug, Journal of Appl. Phys. $\underline{39}$, 4681 (1968).

23. J. Shah, R. F. Leheny, and W. F. Brinkman, Phys. Rev. B $\underline{10}$, 659 (1974).

24. E. A. Meneses, N. Jannuzzi, J. G. Ramos, R. Luzzi, and R. C. Leite, Phys. Rev. B $\underline{11}$, 2213 (1975).

25. J. I. Levatter, R. L. Sandstrom, and Shao-Chi Lin, J. Appl. Phys. $\underline{44}$, 3273 (1973).

26. W. S. Brower, Jr. and H. S. Parker, J. Crystal Growth $\underline{8}$, 227 (1971).

27. P. Y. Yu, Y. R. Shen, Y. Petroff, and L. M. Falicov, Phys. Rev. Lett. $\underline{30}$, 283 (1973).

28. M. V. Klein, Phys. Rev. B $\underline{8}$, 919 (1973).

29. Y. Toyozawa, Progress of Theoretical Physics $\underline{20}$, 53 (1958).

30. J. C. Merle, S. Nikitine, and H. Haken, Phys. Stat. Sol. (b) $\underline{61}$, 229 (1974).

31. S. Nikitine, G. Perney, and M. Sieskind, Comp. Rend. $\underline{238}$, 1987 (1954).

32. For example see C. Kittel, Introduction to Solid State Physics (John Wiley and Sons, Inc., New York, 1971).

33. J. Hallberg and R. C. Hanson, Phys. Stat. Sol. $\underline{42}$, 305 (1970).

PHOTOLUMINESCENCE STUDIES OF THE YELLOW SERIES

FREE EXCITON IN CUPROUS OXIDE USING PULSED

AND CONTINUOUS WAVE TUNABLE DYE LASERS

by

ROBERT M. HABIGER

B.A., Bethany College, 1969

———————————

AN ABSTRACT OF A MASTER'S THESIS

submitted in partial fulfillment of the

requirements for the degree

MASTER OF SCIENCE

Department of Physics

KANSAS STATE UNIVERSITY
Manhattan, Kansas

1975

A pulsed tunable dye laser and a continuous wave tunable dye laser have been used to pump directly the 1S yellow exciton band in Cu_2O. The resulting photoluminescence has been used to infer an effective exciton temperature by making fits to the shape of the phonon-assisted sideband. Hot exciton luminescence has been observed for a wide range of laser frequencies and intensities. For low power density excitation this can be explained by a short exciton lifetime. For high power densities, created by the pulsed laser, there is a relatively strong dependence of the effective exciton temperature on the laser power. This has been attributed to the formation of an exciton subsystem which has reached a quasi-equilibrium via exciton-exciton collisions. Experimental observations and theoretical calculations have been used to make estimates of lifetimes for the free exciton ($\sim10^{-10}$ seconds), for exciton-exciton scattering ($\sim10^{-11}$ seconds), and exciton-acoustic phonon scattering ($\sim6\times10^{-12}$ seconds) which support this model. Exciton temperatures as high as 65K have been obtained for bath temperatures of 20K. An analysis of the Stokes to anti-Stokes ratio indicate an optic phonon temperature rise of less than 17K during the exciton lifetime. A Debye model specific heat calculation is used to also place an upper limit of 34K on the acoustic phonon temperature supporting the view that the power dependence of the exciton temperature is due to exciton-exciton effects and not to phonon heating.